



Resolving volatile sources along the western Sunda arc, Indonesia

Sæmundur A. Halldórsson ^{a,*}, David R. Hilton ^a, Valentin R. Troll ^b, Tobias P. Fischer ^c

^a Fluids and Volatiles Laboratory, Scripps Institution of Oceanography, University of California, San Diego, La Jolla, CA 92093-0244, USA

^b Department of Earth Sciences, CEMPEG, Uppsala University, Villavägen 16, 75236, Sweden

^c Department of Earth and Planetary Sciences, University of New Mexico, Albuquerque, NM 87131-1116, USA

ARTICLE INFO

Article history:

Accepted 15 September 2012

Available online 4 October 2012

Keywords:

Subduction zones

Indonesia

Volatile recycling

Helium isotopes

Carbon isotopes

Nitrogen isotopes

ABSTRACT

We present the chemical and isotope (He–C–N) characterization of active fumaroles and hydrothermal gases and waters from the summits and flanks of 19 volcanic centers along the western Sunda arc, Indonesia. Samples were collected over two field expeditions (1991 and 2010) and cover 13 volcanic centers in Sumatra, 5 in Java and one in Bali. In addition, we present data from three geothermal sites in Sumatra associated with active fault systems in-between volcanic centers (IBVC). The overall aim is to resolve volatiles associated with the sub-arc mantle (subducting slab and mantle wedge) from inputs derived from the over-riding arc crust. The western Sunda arc is a prime locality to assess controls on volatile provenance at subduction zones due to changes in composition and thickness of over-riding crust and variations in sediment input rates along the strike of the arc.

The dry gas chemistry of the majority of volcanic samples is dominated by CO₂ with inert gas variations (He–Ar–N₂) typical of subduction zone gases. However, there is a strong crustal control on the He–CO₂ isotope and relative abundance systematics on a number of volcanic centers: this effect is most clearly observed at flank localities and in water phase samples. Filtering the entire database for modifications due to air contamination, degassing-induced fractionation (C-isotopes and CO₂/³He ratios) and crustal contamination associated with volatile transport within shallow-level hydrothermal systems allows recognition of the magmatic volatile signature of individual volcanoes along the arc. Helium isotopes at all but two volcanic centers (Talang and Dempo on Sumatra) range from 5.3 R_A to 8.1 R_A (R_A = air ³He/⁴He) pointing to the mantle wedge as the principal source of He but with a small input of crustal (radiogenic) He at some localities. Samples from Java and Bali span an even more limited range (6.6 to 7.9 R_A) implying a relatively smaller input of crustal He. Carbon isotope and CO₂/³He ratios vary from –1.4‰ to –6.4‰ and 4.38 to 150 (×10⁹), respectively, with higher and more variable values to the north of Sumatra. This latitudinal effect is not apparent in air-corrected N-isotope values (δ¹⁵N_C = –3.91 to +5.92‰) or various elemental ratios such as N₂/Ar and N₂/He. The three IBVC sites, all located in Sumatra, have significantly lower ³He/⁴He ratios (<3.6 R_A) with CO₂/³He values both higher and lower than volcanic centers. Their δ¹³C, δ¹⁵N_C and gas ratios overlap with the volcanic centers.

The elemental and isotopic characteristics of carbon and helium have been modified at IBVC sites due to crustal processes. However, based upon relationships between CH₄ and ³He as well as co-variations between He–C–N isotopes, the over-riding crust and associated sediments add minimal volatiles to volcanic centers throughout the western Sunda arc. In turn, subducted sediment, particularly the Nicobar Fan which supplies Himalayan-derived sediment to the slab off Sumatra, exerts a strong control on the magmatic CO₂ characteristics although it is less influential for N₂. In spite of large sections of incoming sedimentary material being off-scraped during subduction, our data suggest that a significant fraction must enter the trench, enhancing fluid/melt production in the mantle wedge. We propose that subduction-related source contamination plays the dominant role over thick/old crustal basement in supplying the major volatile output budget of the western Sunda arc.

© 2012 Elsevier B.V. All rights reserved.

1. Introduction

Carbon dioxide and other volatiles erupted at arc volcanoes trace their origins to the mantle wedge, the subducting slab (including

sediments and underlying crust), and the crust through which magmas are erupted (Marty et al., 1989; Poreda and Craig, 1989; Varekamp et al., 1992; Sano and Marty, 1995; van Soest et al., 1998). By resolving contributions from each of these reservoirs to the volcanic arc output, it is possible to constrain the proportion of carbon recycled between trench and arc (shallow recycling) versus the proportion which bypasses the zone of magma generation and

* Corresponding author.

E-mail address: shalldorsson@ucsd.edu (S.A. Halldórsson).

is recycled into the deep mantle (deep recycling) (Hilton et al., 2002).

In this contribution, we present new results on the volatile characteristics of nineteen passively-degassing volcanic centers in the western Sunda arc of Indonesia. Large sections of this arc system, the Sumatra segment in particular, are underlain by thick, Mesozoic continental crust (Hamilton, 1979) composed mainly of granitoids and siliciclastic and carbonate sediments (Hamilton, 1979; Gasparon and Varne, 1995). Gasparon et al. (1994) and Gasparon and Varne (1998) argued that contamination of arc-related magmas by the crust increased in significance from east to west along the Sunda arc, and that the role of subducted sediment on magma chemistry diminished in a complementary fashion. Thus, the western Sunda arc presents a unique test case of volatile provenance associated with arc volcanism, vis-à-vis inputs from the over-riding plate (particularly the crust) versus the subducted slab. Central to this issue, however, is the similar chemical (e.g., trace elements) and radiogenic isotope traits of incoming sediments on the slab and the arc crust itself (Gasparon and Varne, 1998). This also complicates resolution between slab-related volatile additions to the mantle source (primary contamination) and secondary/shallower crustal contamination of magmas en route to the surface.

Coupled studies of He, CO₂ and N₂ (isotopes and relative abundances) can be used in a powerful manner to resolve upper crustal influences and their potential contribution to arc volcanism (e.g., Fischer

et al., 2002; Hilton et al., 2002). Applying such an approach to the western Sunda arc is therefore of great interest given the antiquity and composition of the Sundaland crustal core (Fig. 1) and the presence of well-documented sedimentary provinces on the subducting oceanic parts of the Indo-Australian plate, off-Sumatra and west Java (Moore et al., 1980). In this respect, it is of particular interest to compare the Sumatra segment of the Sunda arc with that of Java/Bali where the over-riding crust is thinner and more oceanic in nature (Hamilton, 1979). Thus, our aim is to identify the various sources contributing to the volatile output in the western Sunda arc and to assess first-order controls on their isotopic and abundance characteristics.

2. Geological setting of the western Sunda arc and the Sumatran segment

Indonesia is one of the most volcano-dense regions on Earth with widespread volcanism resulting from the ongoing subduction of the Indian–Australian Plate beneath the Eurasian Plate (Hamilton, 1979; McCaffrey, 2009) (Fig. 1). The continuous Myanmar–Andaman–Sunda–Banda subduction system makes up the present-day volcanic arc, which has been active since the Cretaceous (Hamilton, 1979). In Indonesia, there are two major crustal regimes which are separated at the Progo–Muria fault zone in central Java (Smyth et al., 2007). The western segment of the Sunda arc consists of Sumatra and west Java where the down-going plate is subducting obliquely beneath

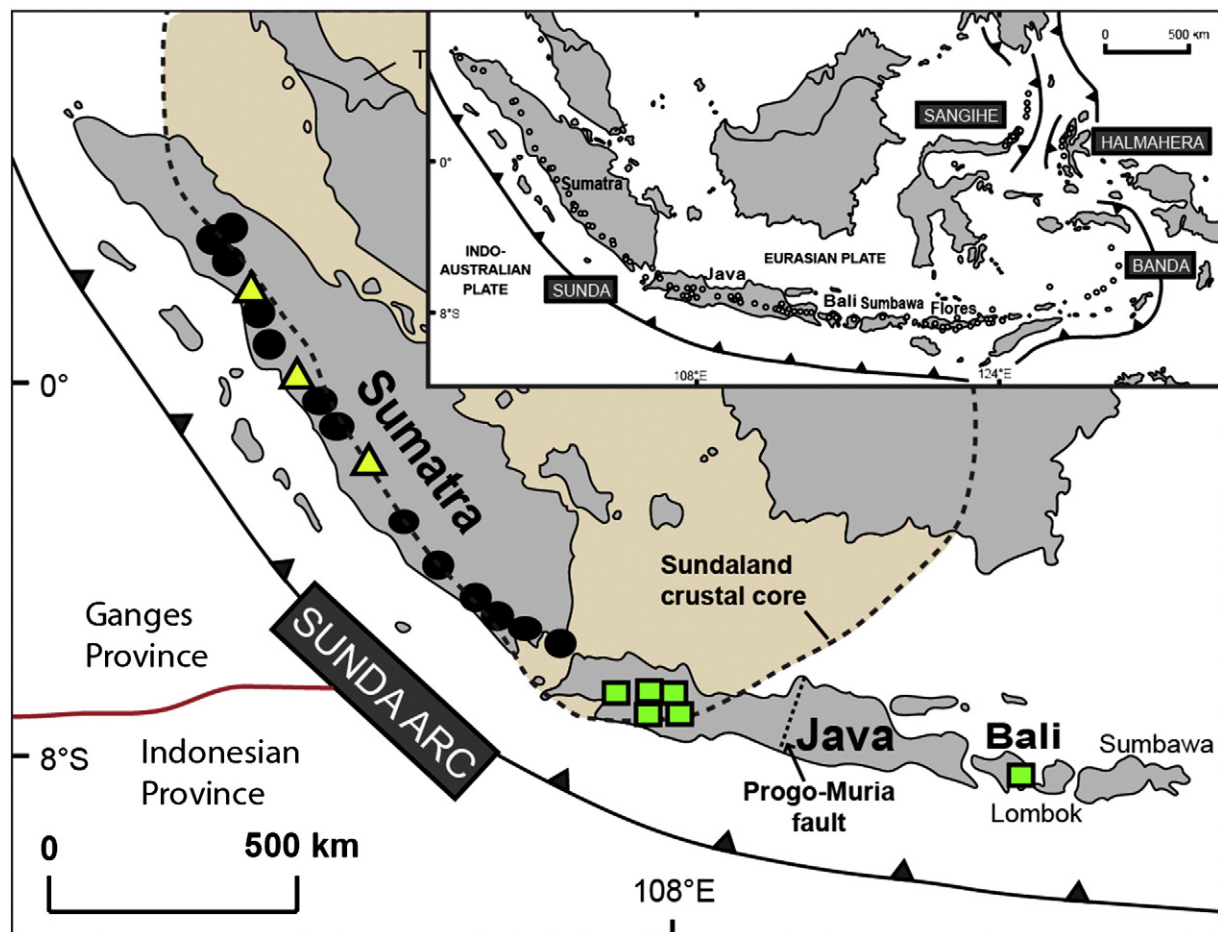


Fig. 1. Map of study area showing the sampling localities (black symbols = Sumatra volcanic centers, yellow triangles = in-between volcanic centers (IBVC) geothermal sites and green boxes = Java/Bali volcanic centers). Sedimentary provinces (Ganges vs. Indonesian) of ocean floor sediments and the Sundaland crustal core are shown for reference. Small inset picture shows the general tectonics of Indonesia, the major plates and arc systems involved. Active and quaternary volcanoes are represented by open symbols (after Gertisser and Keller, 2003).

relatively thick over-riding quasi-continental crust, consisting of the Mesozoic Sundaland core and/or the Sunda Shelf which are composed of continental block fragments. The eastern Sunda and Banda arcs (east Java, Flores, Timor) are built on considerably thinner oceanic crust. In the easternmost part of the arc, the leading-edge of the Australian continent is being subducted (Fig. 1).

The Indo-Australian Plate subducts beneath the Sunda Trench at an orthogonal convergence rate of 50 mm/yr in Sumatra which is considerably lower than ~75 mm/yr in Java and Flores (Von Huene and Scholl, 1991). The age of the subducting lithosphere varies from 50 to 90 Ma from north-to-south along Sumatra and from 100 to 135 Ma from west-to-east in Java (Widiyantoro and van der Hilst, 1996). The dip of the subducting slab changes from ~40° beneath Sumatra to ~60° below Java (Widiyantoro and van der Hilst, 1996). The overall structure and age of the subducting lithosphere strongly influences the style of crustal deformation and associated seismicity along the Sunda arc (Sieh and Natawidjaja, 2000; McCaffrey, 2009). The relatively young age of subducted lithosphere beneath Sumatra has drastic consequences for the depth distribution of earthquake foci, with no earthquakes deeper than ~300 km. In contrast, earthquake focal depths beneath Java extend to the 670 km mantle transition zone (Widiyantoro and van der Hilst, 1996).

Sumatra is situated on the south-western margin of the so-called Sundaland crustal core composed of granitic rocks up to 240 Ma (Gasparon and Varne, 1995). Crustal thickness in Sumatra varies between 25 and 40 km (Sieh and Natawidjaja, 2000; McCaffrey, 2009). During the Triassic to early Jurassic (~250–200 Ma), Sumatra was part of the northern edge of Australia (north of New Guinea) but later rifted from the Australian mainland to form a stable continental margin where it remained until subduction began in the Cretaceous (Hamilton, 1979). The influence of the Sundaland core is clearly evident in the radiogenic isotope systematics of volcanic rocks from Sumatra (e.g., Whitford, 1975). For example, the most radiogenic ⁸⁷Sr/⁸⁶Sr values along the entire Sunda arc are found in lavas of the great Toba eruption in northern Sumatra (Gasparon and Varne, 1998).

The presently-active volcanic front runs parallel to the Sunda Trench along the length of Sumatra, and coincides with the Barisan Mountains and the Sumatran Fault (McCaffrey, 2009). Recent estimates of sediment delivery rates are 83 km³/Myr for Sumatra and 54 km³/Myr for Java (Clift and Vannucchi, 2004). Additionally, a massive accretionary prism has formed offshore Sumatra—forming the Mentawai islands on the fore-arc Simeulue-Enggano ridge, as well as a number of offshore fore-arc basins (Moore and Curray, 1980).

Relatively few petrological and geochemical studies have been reported for Sumatra: however, exceptions include regional studies of Whitford (1975, 1981), Gasparon et al. (1994), Gasparon and Varne (1998) and Turner and Foden (2001). The Toba eruption in northern Sumatra (~75,000 years ago) and the petrology/geochemistry of associated tuffs has been the focus of detailed work (e.g., Chesner et al., 1991; Chesner, 1998; Vazquez and Reid, 2004).

3. Sampling and analytical techniques

Sampling of the western Sunda arc was undertaken in two field expeditions—in 1991 and 2010. In the 2010 expedition, we collected 35 geothermal fluid samples (including 17 duplicates) from 16 localities along a ~2000 km transect of Sumatra, from Rajabasa volcano in the south to Sibayak volcano in the north (see Budd et al., 2012a and Fig. 1). Sampling included the following historically-active stratovolcanoes (from south to north): Dempo, Kaba, Talang, Marapi, Sorik Marapi, Singabung, and Sibayak as well as Rajabasa, Sekincau, and Bual Bauali volcanoes where there is no historical record of eruptive activity (Gasparon, 2005). Three sampling localities are associated with massive caldera-forming lakes and/or caldera floors: Semining (Ranau caldera) and Panururan (Toba caldera) and the Ratai hydrothermal field by the Hulubelu caldera (Gasparon, 2005). These 13 volcanic

centers, which are all passively-degassing, were supplemented by in-between volcanic center (IBVC) geothermal sites associated with active fault systems: from south to north, the Dusan Baru field near Kerinci volcano, the Rimbo Panti field adjacent to Talakmau volcano, and the Helatoba–Tarutung fumarole field. We also collected gas samples from the historically-active Tangkuban Parahu volcano on Java.

The 1991 expedition included Sumatra (including many of the same sampling sites visited in 2010) in addition to five volcanic centers on Java and the island of Bali. With the exception of Talagabodas, all of the volcanoes from Java and Bali (Guntur, Papandayan, Galunggung and Batur) are known to be historically-active. Results of the earlier study helped direct sampling in the 2010 expedition and provided a useful perspective on temporal changes at individual sites over a two-decade period. Thus, the entire sample set (39 gas phase samples and 23 water phase samples) is composed of summit fumaroles (100 °C) from Marapi, Sibayak, Singabung and Papandayan volcanoes, which are classified as volcanic fluids (e.g., Taran and Giggenbach, 2003). The remaining samples are classified as hydrothermal fluids as they were sampled from volcano flanks and/or IBVC. In total, fluid samples were collected from (i) 9 fumaroles, (ii) 12 bubbling acid springs, (iii) 11 hot water springs, making a total of 56 samples (with duplicates) from 32 individual localities on Sumatra. Additionally, 4 fumaroles and 2 water springs from 6 different localities were sampled along the Java/Bali segment (see Table 1).

Sampling protocols and analytical procedures adopted during the 1991 expedition follow closely those described in Hilton et al. (1993). The 2010 samples were similarly collected in evacuated low-He diffusivity glass flasks (1720- or AR-glass) and/or annealed copper tubes, with adoption of the inverted funnel method to collect gas phase samples. Evacuated ~200 mL pyrex flasks, aka Giggenbach bottles, were used for major gas chemistry (2010) or an aliquot was prepared from the AR-glass bottles (1991 expedition).

Analytical protocols for the 2010 samples follow closely those described by Shaw et al. (2003) and Ray et al. (2009). Briefly, samples were released into an ultra high vacuum (UHV) stainless steel purification line where non-condensable gases (He–Ne–N₂) were cryogenically separated from condensable gases (H₂O and CO₂). The light noble gases (He–Ne) were then isolated from the active and heavy noble gas fraction by exposure to an activated charcoal trap at –196 °C and a Ti-getter held at 700 °C, with a calibrated aliquot (~0.5%) transferred to a MAP-215 noble gas mass spectrometer for He isotopic and He/Ne relative abundance analysis. Calibrated aliquots of air, run under identical conditions to samples, were used to gauge mass fractionation and to assess machine sensitivity.

The condensable gas fraction (CO₂) was isolated from water vapor and transferred to a dedicated Pyrex-glass vacuum line for further purification and manometric measurement in a calibrated volume to obtain the total abundance of CO₂. Following measurement, the CO₂ was split and transferred in Pyrex® glass breakseal to a Thermo-Finnigan Delta^{Plus}XP isotope ratio mass spectrometer for δ¹³C analysis.

During the course of this study, a new protocol was developed for N₂ isotope measurement of gas and fluid samples. An additional aliquot of gas was collected in a Pyrex glass breakseal on the stainless steel extraction line without exposure to either the charcoal trap or Ti-getter. The aliquot was then transferred to a dedicated N-purification line attached to a static noble gas mass spectrometer (VG5440; Craig et al., 1993). A description of the purification system to prepare the samples for N-isotope measurement is given by Barry et al. (2013–this issue). Briefly, the bulk gas in the breakseal was expanded into the line where residual condensable gases were isolated using a cold finger held at liquid-nitrogen temperature. Gases were then exposed to hot (850 °C) CuO for 10 min in the presence of a Pt-foil catalyst, held at 1000 °C, to enhance the reaction between O₂ and carbonaceous (CO, C₂H₄) and nitrogenous (NO) species, to CO₂ and NO₂, respectively. Excess oxygen was then reabsorbed back onto the CuO finger in two steps, first at 600 °C and then at 450 °C. Throughout the process, the condensable

Table 1
Helium, carbon and nitrogen isotope and relative abundance characteristics of geothermal fluids from Sumatra, Java and Bali.

Location ^a	Sample ID ^b	Sample Type ^c	Latitude (S/N)	Longitude (E)	T (°C)	³ He/ ⁴ He	X ^e	³ He/ ⁴ He	CO ₂ / ³ He (×10 ⁹)	δ ¹³ C (CO ₂) (‰)VPDB	δ ¹⁵ N (N ₂) (‰)AIR	δ ¹⁵ N (N ₂) (‰)C AIR ^g	[⁴ He] _c cm ³ STP/ gH ₂ O (×10 ⁻⁹) ^{h,i}
						R _M /R _A ^d		R _C /R _A ^f					
<i>Sumatra—volcanoes</i>													
Rajabasa	SUM10-2	G-as	S 05°44'53.6"	105°36'58.3"	32	8.05	252	8.08	9.33	-3.0	3.48	3.49±0.46	
	SUM10-3	W-fs	S 05°45'07.0"	105°38'03.0"	54	3.46	6.52	3.91	1023	-4.1	nd	nd	62.8
	725	W-fs	S 05°45'07"	105°38'03"	58	5.52	9.33	6.06	2003	-4.7	nd	nd	4.3
	681	W-fs	S 05°44'54"	105°36'58"	65	3.37	1.77	6.45	724	-2.3	nd	nd	6.7
	726	W-fs				3.03	1.61	6.37	665	-2.7	nd	nd	9.5
Ratai (Hulubelu)	SUM10-4	G-as	S 05°19'53.5"	104°34'22.9"	86	5.25	7.66	5.88	5.03	-3.7	1.55	1.63±0.36	
	SUM10-6	G-as				5.48	9.19	6.02	4.38	-4.5	0.79	0.76±0.74	
Sekincau	SUM10-5	G-as	S 05°05'21.2"	104°18'26.3"	101	5.93	60.1	6.01	9.60	-4.8	4.13	4.18±0.30	
	SUM10-7	G-as				5.46	24.3	5.65	9.00	-4.2	1.52	1.54±0.40	
	694	G-as	S 05°05'21"	104°18'26"	27	6.41	7.97	7.19	75.3	-3.4	nd	nd	
Seminung	746	G-as				6.33	8.11	7.08	70.4	-3.4	nd	nd	
	SUM10-8	W-fs	S 04°52'38.9"	103°55'54.0"	58	3.50	5.59	4.04	229	-8.9	nd	nd	106
	SUM10-9	W-fs				2.49	3.80	3.02	210	-6.2	4.01	5.08±0.51	167
	690	W-fs	S 04°52'39"	103°55'54"	59	2.53	1.37	6.69	141	-6.3	nd	nd	30.8
Dempo	649	W-fs				2.6	1.32	7.22	169	-6.3	nd	nd	32.5
	SUM10-10	W-fs	S 04°10'01.1"	103°04'04.6"	95	1.28	4.57	1.35	200	-3.2	-0.06	-0.36±0.47	52.0
	SUM10-14	W-fs				1.00	2.62	1.00	16.7	-9.6	nd	nd	470
	705	W-fs	S 04°10'01"	103°04'05"	92	2.06	87.2	2.08	70.6	nd	nd	nd	255
Kaba	756	W-fs				2.06	65.2	2.08	63.2	nd	nd	nd	302
	SUM10-11	W-fs	S 03°27'41.2"	102°34'10.7"	48	6.27	27.5	6.47	59.2	-6.9	5.74	5.92±0.43	713
	SUM10-12	W-fs				5.79	15.1	6.13	60.6	-8.2	nd	nd	765
Talang	SUM10-15	W-fs	S 00°55'03.5"	100°40'50.9"	45	1.66	3.35	1.95	442	-5.6	3.88	5.11±0.48	93.1
	SUM10-17	W-fs				1.56	3.37	1.80	471	-4.7	nd	nd	104
Marapi	SUM10-18	G-sf	S 00°23'16.9"	100°27'38.7"	89	6.97	1265	6.98	11.4	-2.6	-2.07	-2.07±0.46	
	SUM10-20	G-sf				7.09	319	7.11	14.1	-1.4	-2.17	-2.18±0.28	
	674	G-sf	S 00°23'17"	100°27'39"	92	6.15	23.5	6.38	22.5	-2.4	nd	nd	
	680	G-sf				6.47	662	6.48	23.3	-2.6	nd	nd	
Sorik Marapi	SUM10-22	G-ff	N 00°42'09.2"	099°33'46.2"	59	5.64	10.2	6.14	38.4	-5.3	2.29	2.43±0.53	
	SUM10-23	G-ff				6.69	57.8	6.79	40.6	-6.4	4.08	4.13±0.38	
	SUM10-27	G-as	N 00°42'20.4"	099°34'43.0"	94	3.46	203	3.47	16.2	-5.3	1.48	1.48±0.36	
	Cu-tube-2	G-as				2.89	21.5	2.99	27.1	-3.8	0.15	0.11±0.41	
	701	G-ff	N 00°42'09"	099°33'46"	88	6.52	65.8	6.6	32.5	-3.0	nd	nd	
Bual Buali	565	G-as	N 00°42'20"	099°34'43"	90	3.32	40.8	3.38	34.4	nd	nd	nd	
	741	G-as				3.33	22.7	3.46	53.3	-3.1	nd	nd	
	SUM10-24	G-ff	N 01°33'59.4"	099°16'05.2"	92	5.92	20.1	6.18	16.3	-1.4	-3.38	-3.61±0.53	
	SUM10-25	G-ff				1.08	2.80	1.12	60.9	-2.8	-2.16	-3.91±0.59	
	615	G-ff	N 01°33'59"	099°16'05"	94	6.47	73.0	6.55	25.8	nd	nd	nd	
Panururan	675	G-ff				6.51	88.7	6.58	27.3	-5.3	nd	nd	
	SUM10-29	G-as	N 02°37'06.6"	098°40'22.7"	62	1.80	4.47	2.03	21.5	-1.6	0.27	0.06±0.64	
	SUM10-30	G-as				5.29	253	5.30	36.9	-2.3	3.76	3.77±0.53	
	665	G-as	N 02°37'07"	098°40'23"	60	5.06	160	5.08	56.8	-4.6	nd	nd	
Singabung Sibayak	734	G-sf	N 03°10'0"	098°23'30"	120	5.98	34.0	6.14	150	-3.7	nd	nd	
	SUM10-26	G-sf	N 03°14'22.9"	098°30'16.5"	95	6.74	1863	6.74	5.74	-3.8	4.33	4.33±0.38	
	SUM10-28	G-sf				6.74	292	6.76	5.96	-2.8	5.52	5.54±0.36	
	Cu-tube-5	W-fs	N 02°57'40.9"	098°52'31.0"	64	4.64	5.36	5.47	46.9	-3.7	nd	nd	19.0
	Cu-tube-6	W-fs				6.40	45.6	6.52	54.5	-4.1	nd	nd	11.9
	Cu-tube-7	W-fs				6.11	24.2	6.33	43.1	-4.0	nd	nd	15.5
	667	W-fs	N 02°57'41"	098°52'31"	44	6.31	7.22	7.17	12.0	-3.9	nd	nd	
733	G-sf	N 03°14'23"	098°30'17"	106	6.68	1431	6.68	11.5	nd	nd	nd		
<i>Sumatra—IBVC^a</i>													
Dusan Baru	SUM10-13	G-as	S 01°59'18.9"	101°21'28.1"	58	2.02	437	2.03	14.2	-6.7	3.49	3.50±0.38	
	SUM10-16	G-as				2.00	394	2.00	14.0	-8.0	3.25	3.26±0.55	
	731	W-as	S 01°59'19"	101°21'28"	94	2.03	15.1	2.10	279	-5.6	nd	nd	67.8
Rimbo Panti	SUM10-19	G-as	N 00°20'52.6"	100°04'06.9"	92	3.62	295	3.62	0.38	-4.9	1.75	1.75±0.38	
	SUM10-21	G-as				3.71	312	3.72	nd	nd	1.83	1.83±0.32	
<i>Sumatra—IBVC^a</i>													
Helatoba—Tarutung	Cu-tube-3	G-as	N 02°04'31.0"	098°56'39.5"	63	1.71	38.7	1.73	1107	-2.1	-0.90	-0.95±0.48	
	Cu-tube-4	G-as				1.62	38.6	1.64	1505	-1.8	-0.54	-0.58±1.19	

gases (mostly CO₂, SO₂ and H₂O) were adsorbed onto a cold finger held at liquid nitrogen temperature. The purified N₂ was then expanded into a VG-5440 mass spectrometer where the ratio of ¹⁵N to ¹⁴N was analyzed by measuring m/z ratios of 28, 29, and 30, allowing calculation of the N-isotope ratio (δ¹⁵N) and application of a comprehensive CO correction to all samples (Barry et al., 2012). Hydrocarbon interferences at masses 28 and 29 are considered negligible. An internal pure N₂ standard, calibrated relative to Scripps-pier air, was repeatedly

measured throughout the 23-day run of the western Sunda sample set. In addition, repeated measurements (n = 6) of the Scripps-pier air standard during these runs, following exactly the same analytical protocol as samples, allowed evaluation of uncertainties associated with both sample preparation and mass spectrometer measurement. We take the average reproducibility of our in-house air standard δ¹⁵N value of ±0.26‰ (1σ) as the best estimate of the external reproducibility of our nitrogen system. Throughout the sample runs, procedural N₂ blanks

Table 1 (continued)

Location ^a	Sample ID ^b	Sample Type ^c	Latitude (S/N)	Longitude (E)	T (°C)	³ He/ ⁴ He		CO ₂ / ³ He (×10 ⁹)	δ ¹³ C (CO ₂) (‰)VPDB	δ ¹⁵ N (N ₂) (‰)AIR	δ ¹⁵ N (N ₂) (‰) _c AIR ^g	[⁴ He] _c cm ³ STP/ gH ₂ O (×10 ⁻⁹) ^{h,i}
						R _M /R _A ^d	X ^e					
<i>Java—volcanoes</i>												
Tangkuban Parahu	SUM10-1	G-sf	S 06°45'41.2"	107°37'32.9"	51	7.91	338	7.93	13.8	-5.2	1.6	1.6 ± 0.54
Guntur	721	G-ff	S 07°8'36"	107°50'23"	98	6.75	58.1	6.85	16.4	-2.4	nd	nd
Papandayan	696	G-sf	S 07°18'53"	107°43'57"	105	6.61	851	6.62	28.2	nd	nd	nd
Galunggung	711	W-fs	S 07°15'0"	108°3'30"	48	5.44	3.68	7.10	172	-5.5	nd	32.48
Talagabodas	673	G-ff	S 07°12'30"	108°4'0"	95	7.68	1144	7.69	20.2	nd	nd	nd
<i>Bali—volcano</i>												
Batur	724	W-fs	S 08°15'03"	115°24'03"	32	6.81	6.45	7.87	25.2	nd	nd	200

nd = not determined.

^a Sample locations given from south to north. IBVC = In-Between Volcanic Centers.

^b SUM10- and Cu-tube- sampled in October/November 2010, GPS datum WGS84; numbers sampled February/March 1991, map coordinates.

^c Abbreviations: G = gas; W = water; sf = summit fumarole; ff = flank fumarole; as = gas from acid spring; fs = flank spring.

^d R_M/R_A notation where R_M = sample ³He/⁴He ratio and R_A = atmosphere ³He/⁴He ratio (= 1.4 × 10⁻⁶).

^e X = (⁴He/²⁰Ne)_M / (⁴He/²⁰Ne)_{air} × βNe/βHe, where M is the measured ⁴He/²⁰Ne ratio, β represents the Bunsen solubility coefficient assuming a recharge temperature of 15 °C (Weiss, 1971).

^f R_C/R_A is the air-corrected He isotope ratio = [(R_M/R_A × X) - 1] / (X - 1).

^g δ¹⁵N (N₂) (‰)_c is the air-corrected N isotope ratio = [(δ¹⁵N × X) - 1] / (X - 1). See appendix.

^h Helium abundance data are corrected for air contamination where [He]_c = ([He]_M × (X - 1)) / X.

ⁱ All errors are reported at the 1σ level; R_C/R_A uncertainty is estimated ± 3%, CO₂/³He uncertainty is estimated ± 5%, δ¹³C uncertainty is estimated < ± 0.5%, [⁴He]_c is estimated at ± 5%.

where monitored prior to each sample analysis. Except for two samples (from Helatoba-Taratunga, blank ~9%), blank contributions were always less than 5% of sample yields and less than 2% in most cases.

Major gas chemistry of the 2010 samples was measured by a GC-quadrupole system at UNM. In this system, CO₂, N₂, Ar + O₂, CH₄, and CO are measured on a Gow Mac Gas Chromatograph with Discharge Ionization Detector (DID) [Heyesep and MolSieve columns]. The Ar and O₂ concentrations are measured on a Pfeiffer quadrupole mass spectrometer in dynamic mode. Major gas chemistry of samples from the 1991 expedition (listed in Table 2, identified with numbers only) was measured in the same laboratory using methods outlined previously (Zimmer et al., 2004; Elkins et al., 2006). For that system, samples with very high O₂ concentrations are likely to yield unreliable Ar data due to the difficulty of separating Ar and O₂ in a saturated O₂ separation column (see discussion in Zimmer et al., 2004 and Elkins et al., 2006). Two samples reported in Table 2, shown in italics and underlined, have unusually low N₂/Ar ratios (Seminung = 14.8 and Dempo = 14.6) and are not included in the following discussion.

4. Results

We report ³He/⁴He, CO₂/³He, C- and N-isotopes, and He abundance results (water phase only) in Table 1 with the major gas chemistry in Table 2. Sample locations are given in Fig. 1, with a filtered version of the dataset (see Section 5.2) plotted as a function of latitude in Figs. 6 to 8.

4.1. Major gas chemistry

The majority of samples is dominated by CO₂ with 34 out of 39 gases and waters having over 80% (dry gas) CO₂ (Table 2). The only localities showing considerably lower CO₂ content are the IBVC Rimbo Panti hydro-thermal site where N₂ dominates the dry gas budget (~58%) and Ratai (~72%). Nitrogen is the most abundant gas among the non-condensable gases but, with the exception of Rimbo Panti and Ratai, is always less than 15% of the total gas budget. Only three localities (Sorik Marapi, Pangururan and Tangkuban Parahu) show hydrogen concentrations higher than 1%, whereas only four of 21 localities (Sorik Marapi, Ratai, Seminung, and Marapi) have greater than ~5% oxygen. Methane is variable but the majority of samples contain less than 1% methane. However, two IBVC hot spring localities, Dusan Baru and

Rimbo Panti, have significant amounts of CH₄ (~5% and ~7%, respectively). We also note the relatively high CH₄ (1.5%) at the Sorik Marapi flank locality. Notably, all three of these localities are characterized by relatively low ³He/⁴He ratios (2.1 R_A to 3.7 R_A).

In addition to these general features of the major gas chemistry, we use the ternary N₂–He–Ar inert gas plot (Fig. 2) to distinguish between “mantle-derived” and “arc-type” gases (after Giggenbach, 1996). Arc-related geothermal fluids tend to have high N₂/He (>1000) and N₂/Ar (>83) when compared to mantle-derived fluids as a result of addition of sedimentary-derived nitrogen from the subducting slab (e.g., Giggenbach, 1996). Most samples of the present study fall within the field of arc-related gases but with some notable exceptions: i) gas phase samples from Rimbo Panti (RP) and Sibayak (SII) and water phase samples from Batur (B) have low N₂/Ar ratios and thus fall below the field for mantle-derived gases, ii) samples from Sorik Marapi (SM1), Helatoba-Taratunga (HT) and Ratai (R) all have very high ratios of N₂/He (>10,000), iii) samples from Guntur (G), Sorik Marapi (SM) and Singabung (S) all fall outside the proposed field for arc- and mantle-derived fluids, iv) a few samples (e.g., Pangururan and Sibayak) have N₂–He–Ar systematics consistent with mantle-derived gases.

4.2. ³He/⁴He ratios and dissolved helium in water spring samples

Helium isotope results for 32 localities on Sumatra and 6 on Java/Bali are given in Table 1. We plot all measured He isotopes (R_M/R_A) (including duplicates) versus solubility-corrected, air-normalized He/Ne ratio (X) to assess the integrity of the He isotope results (Fig. 3a). Measured ³He/⁴He ratios (reported as R_M/R_A where R_M = measured ³He/⁴He of sample and R_A = ³He/⁴He of air; 1.4 × 10⁻⁶) have been corrected (to R_C/R_A) for the presence of atmospheric components using the air-normalized He/Ne ratio multiplied by the ratio of the Bunsen coefficients, assuming an air-equilibration temperature of 15 °C (= X value—see Table 1 footnote for details plus an estimate of the analytical uncertainty). For the most part, the correction results in only minor (<0.3 R_A) changes to the measured ³He/⁴He (R_M/R_A) ratio. However, where X values are low (<2), correction to measured values can be large, up to 3.1–4.6 R_A for two water samples (Rajabasa and Seminung). We note also that agreement between duplicate samples generally falls within 0.5 R_A; however, 13 of 24 duplicates agree within 0.1 R_A. In contrast, some samples show poor agreement e.g., Sibayak (5.5 R_A vs. 6.5 R_A), Bual Bual (1.1 R_A

Table 2
Gas chemistry of geothermal fluids from Sumatra, Java and Bali (vol.% dry gas).

Location	Sample ID ^a	Type ^b	CO ₂	He [ppm] ^c	H ₂	Ar ^d	O ₂	N ₂	CH ₄	N ₂ /Ar	N ₂ /He	CH ₄ / ³ He ($\times 10^7$)
<i>Sumatra—volcanoes</i>												
Rajabasa	G-SUM10-1	G-as	91.86	8.70	nd	0.023	0.29	7.38	0.46	318	8478	4.63
	725	W-fs	99.96	0.077	nd	nd	nd	0.036	nd	nd	4675.3	nd
	681	W-fs	99.79	0.12	nd	nd	nd	0.21	nd	nd	17500	nd
	726	W-fs	99.64	0.17	nd	nd	nd	0.36	nd	nd	21176	nd
Ratai (Hulubelu)	G-SUM10-3	G-as	12.92	3.12	0.0010	0.61	14.0	72.4	0.049	118	232280	1.87
Sekincau	G-SUM10-4	G-as	89.64	11.1	0.16	0.11	1.03	8.44	0.61	74.3	7610	6.55
	694	G-as	99.17	1.31	nd	0.011	nd	0.79	0.04	70.1	6031	2.79
	746	G-as	94.79	1.36	nd	0.010	4.41	0.75	0.04	76.0	5515	2.70
Seminung	690	W-fs	72.01	0.55	nd	<u>0.034</u>	26.8	0.51	nd	<u>14.8</u>	9273	nd
	649	W-fs	98.85	0.58	nd	0.019	nd	1.13	nd	58.0	19483	nd
Dempo	705	W-fs	93.62	4.56	nd	<u>0.41</u>	nd	5.93	0.040	<u>14.6</u>	13004	3.03
	756	W-fs	99.22	5.40	nd	nd	nd	0.78	nd	nd	1444	nd
Marapi	674	G-sf	72.23	3.59	nd	nd	26.7	0.56	nd	nd	1560	nd
	680	G-sf	99.97	4.73	nd	nd	nd	0.032	nd	nd	67.7	nd
Sorik Marapi	G-SUM10-9	G-as	81.63	10.4	5.18	0.012	1.60	10.08	1.50	875	9727	29.7
	G-SUM10-10	G-ff	84.36	2.56	0.0070	0.019	2.04	13.48	0.091	694	52748	3.76
Bual Buali	701	G-ff	99.87	3.32	nd	0.0015	nd	0.13	0.0007	87.5	392	0.024
	565	G-as	89.99	5.54	nd	0.014	9.18	0.78	0.055	55.3	1408	2.09
	741	G-as	99.08	3.86	nd	0.00033	0.66	0.23	0.046	703	596	2.49
	G-SUM10-11	G-ff	91.77	6.51	0.076	0.027	2.45	5.20	0.47	195	7999	8.39
Pangururan	615	G-ff	99.98	4.22	nd	nd	nd	nd	0.019	nd	nd	0.49
	675	G-ff	99.00	3.94	nd	nd	nd	0.98	0.019	nd	2487	0.52
	G-SUM10-13	G-as	92.29	3.37	3.66	0.0025	0.98	2.55	0.52	1022	7569	20.80
Singabung	665	G-as	99.88	2.47	nd	0.0022	nd	0.1	0.017	46.2	405	0.94
	734	G-sf	99.91	0.78	nd	0.00086	nd	0.095	nd	110	1218	nd
Sibayak	G-SUM10-15	G-sf	97.23	17.9	0.0060	0.00011	0.61	1.96	0.17	17083	1091	1.02
	G-SUM10-16	G-sf	96.59	17.1	0.011	0.00016	0.45	2.64	0.31	16469	1544	1.89
	733	G-sf	99.96	9.30	nd	0.00086		0.035	0.007	40.6	37.6	0.076
<i>Sumatra—IBVC</i>												
Dusan Baru	G-SUM10-5	G-as	81.30	20.2	0.029	0.21	0.47	11.60	6.39	55.2	5746	112
	G-SUM10-6	G-as	79.98	20.4	0.019	0.098	1.00	11.93	6.95	122	5847	122
	731	W-as	99.54	1.21	nd	nd	nd	0.43	0.028	nd	3554	7.80
Rimbo Panti	G-SUM10-7	G-as	30.14	156	0.0031	1.80	5.05	57.86	5.14	32.2	3701	6.48
	G-SUM10-8	G-as	30.52	156	0.0021	1.77	3.93	58.22	5.52	32.9	3724	6.79
Helatoba–Tarutung	G-SUM10-12	G-as	98.81	0.37	0.054	0.0014	0.32	0.74	0.075	534	20159	84.10
<i>Java—volcanoes</i>												
Tangkuban Parahu	G-SUM10-2	G-sf	86.05	5.62	8.15	0.0013	0.56	5.08	0.16	3894	9034	2.62
Guntur	721	G-ff	96.94	5.46	nd	0.00030	2.83	0.17	0.005	573	311	0.10
Galunggung	711	W-fs	99.87	0.58	nd	nd	nd	0.13	nd	nd	2241	nd
Talagabodas	673	G-ff	99.97	4.59	nd	nd	nd	0.033	nd	nd	71.9	nd
<i>Bali—volcano</i>												
Batur	724	W-fs	99.08	3.57	nd	0.023	nd	0.9	nd	38.3	nd	nd

nd=not determined.

^a G-SUM10- samples were analyzed with an updated GC system at UNM whereas samples listed with numbers only were analyzed on the old GC system in the same lab.

^b Abbreviations: G = gas; W = water; sf = summit fumarole; ff = flank fumarole; as = gas from acid spring; fs = flank spring.

^c Helium conc. are calculated from the ³He/⁴He ratios, CO₂/³He ratios and the CO₂ vol.% dry gas.

^d Underlined values in italics have been removed from the discussion as the Ar data are not considered reliable.

vs. 6.2 R_A) and Panururan (2.0 R_A vs. 5.1 R_A). We note that the X values for some of these samples are exceptionally low and thus these samples have experienced significant atmospheric contamination (see discussion in Section 5.1.1).

Helium isotope (³He/⁴He) values vary considerably along the western Sunda arc, from 1.0 R_A to 8.1 R_A (Table 1), and thus demonstrate a significant contribution of mantle-derived helium, from 13% to 100% (assuming a binary mixing between MORB (8 R_A) and crustal component (–0.01 R_A)). The majority of fluid samples from volcanic centers in Sumatra have ³He/⁴He ratios in the range 5.0 to 7.2 R_A, typical of arcs worldwide (Hilton et al., 2002). The one exception is Rajabasa (south Sumatra) where ³He/⁴He is coincident with MORB (8.1 R_A). Significant additions of radiogenic helium ($\gg 50\%$ using the same end-members and assuming a binary mixture as above) are found in geothermal fluids from the flanks of Rajabasa (3.9 R_A, 1 sample), Seminung (3.0–4.0 R_A, 2 samples), Dempo (1.0–2.1 R_A, 4 samples), Talang (1.8–2.0 R_A, 2 samples) and Sorik Marapi (3.0–3.5

R_A, 4 samples). Of these, only Dempo and Talang do not show correspondingly higher ³He/⁴He ratios from different flank and/or summit fumaroles. Radiogenic He additions are also evident in two gas phase samples from Ratai hydrothermal field near Hulubulu caldera (6.0 R_A).

Fluids from hydrothermal sites associated with fault systems which lie between volcanic centers (IBVC) tend to also show significant radiogenic additions, e.g., Dusan Baru (2.1 R_A, 3 samples), Rimbo Panti (3.6 R_A, 2 samples) and Helatoba–Tarutung (1.7 R_A, 2 samples). Other general features of the He isotope results is that the Java and Bali samples show little evidence for significant radiogenic additions, and span a limited range of 6.6 to 7.9 R_A. Finally, there are not significant differences in He isotope systematics between different sample types (gas versus water phase) from the same locality (e.g., Sibayak, Dusan Baru).

The measured dissolved helium abundances in water spring samples (n=22) are corrected for atmospheric He and reported in Table 1. They range from 11.9 to 765 ncm³ STP/gH₂O. Thermal springs from the flanks of Kaba volcano show the highest helium contents

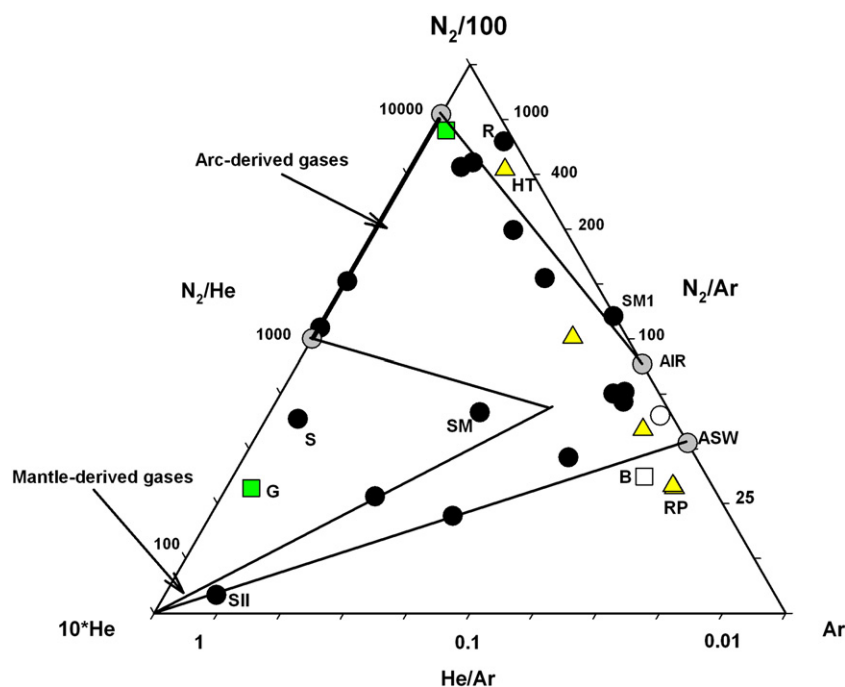


Fig. 2. Ternary plot of the non-reactive gases He–N₂–Ar. The fields for mantle-derived and arc-type gases, as well as N₂–Ar ratio of air (83) and air-saturated groundwater (ASW-45) are shown (after Giggenbach, 1996). See text for details on sample identity. Gas phase samples (closed symbols) and water phase samples (open symbols) from volcanic centers on Sumatra are separated from samples collected in-between volcanic centers (IBVC) (yellow triangles). Samples from Java/Bali are shown as boxes: green boxes for gas phase and open boxes for water phase samples.

and they also have amongst the highest ³He/⁴He ratios for the water samples (6.1–6.5 R_A). The Kaba springs also had one of the lowest measured temperatures (48 °C).

4.3. δ¹³C (CO₂) values

The δ¹³C (CO₂) values of all gas and water phase samples (including duplicates) are shown in Fig. 4 (plotted vs. CO₂/³He). The δ¹³C values range from –1.4‰ to –9.7‰ with only 6 of 53 samples showing values lower than the mean MORB value of –6.5‰ (Sano and Marty, 1995). Amongst the gas phase samples, only samples from the Dusan Baru hydrothermal area (Kerinci Valley) show low δ¹³C values (–6.7 to –8.0‰) whereas the lowest value is found in a water phase sample from Dempo (–9.7‰). The highest observed values are –1.4‰ in flank fumaroles at Bual Buali and summit fumaroles at Marapi. Water phase samples do not demonstrate systematically different δ¹³C values compared to gas samples: water samples vary from –2.3‰ to –9.7‰ whereas gas phase samples vary from –1.4 to –8.0‰. In contrast to He isotopes, the C isotope values observed at IBVC locations show good correspondence with values from the volcanic centers.

4.4. CO₂/³He ratios

The molar ratio of CO₂/³He varies by over 4 orders of magnitude for the western Sunda arc samples (Fig. 4), from ~0.4 × 10⁹ to ~2 × 10¹² and are thus, with the exception of one sample from Rimbo Panti (0.38 × 10⁹), higher than the global mean for MORB (2 × 10⁹) (Marty and Jambon, 1987). Indeed, the majority of samples have ratios greater than the mean value for worldwide arcs (16 ± 11 × 10⁹) (Sano and Williams, 1996). In contrast to He and C isotopes, water phase samples have significantly higher CO₂/³He ratios relative to corresponding gases (Fig. 4), presumably because gas samples are less likely than waters to experience elemental fractionation (see Section 5.1.2).

Two samples clearly stand out from the general range of 4.4–150 (× 10⁹) observed for gas phase samples: Rimbo Panti acid spring (0.38 × 10⁹) and Helatoba–Tarutung hydrothermal area (1107–1505 (× 10⁹)). Notably, both these localities are at a considerable distance from volcanic centers. In contrast, the Dusan Baru hydrothermal site agrees well with ratios generally observed at volcanic centers. Finally, with the exception of the water sample from Galunggung (172 × 10⁹), the Java/Bali samples show a limited range of ratios—14–28 (× 10⁹), coincident with the global mean for arcs worldwide (16 × 10⁹).

4.5. δ¹⁵N (N₂) values

In Fig. 3b, we plot measured δ¹⁵N versus the air-normalized He/Ne ratio (X value—see section 4.2 and Table 1 footnote for details). The measured nitrogen isotope data from the 2010 sampling campaign (which includes one value from Tangkuban Parahu on Java) ranges from –3.38‰ to +5.74‰ (Fig. 3), with the majority of samples displaying values greater than air - consistent with values found previously at other arc-related volcanoes (up to +7‰, e.g., Sano et al., 1998; Fischer et al., 2002; Clor et al., 2005; Elkins et al., 2006; Mitchell et al., 2010). Four samples show isotope values identical to that of air.

Measured δ¹⁵N values (reported as δ¹⁵N in Table 1) have been corrected for the presence of atmospheric nitrogen using an approach similar to that used for He isotopes: in the following discussion, we use the air-corrected δ¹⁵N ratio (δ¹⁵N_C) based upon this correction. However, an alternative approach to account for air-derived N₂ is based upon measured N₂/He ratios (e.g., Fischer et al., 2002). In the Appendix A, we contrast these two approaches specifically for our dataset.

The most positive δ¹⁵N_C values for our dataset are for a water sample from Kaba volcano (5.92‰) and a summit gas samples from Sibayak volcano (5.54‰). Bual Bual volcano has the lowest (duplicate) values in the dataset: –3.61‰ and –3.91‰. Along with Marapi (–2.07 and

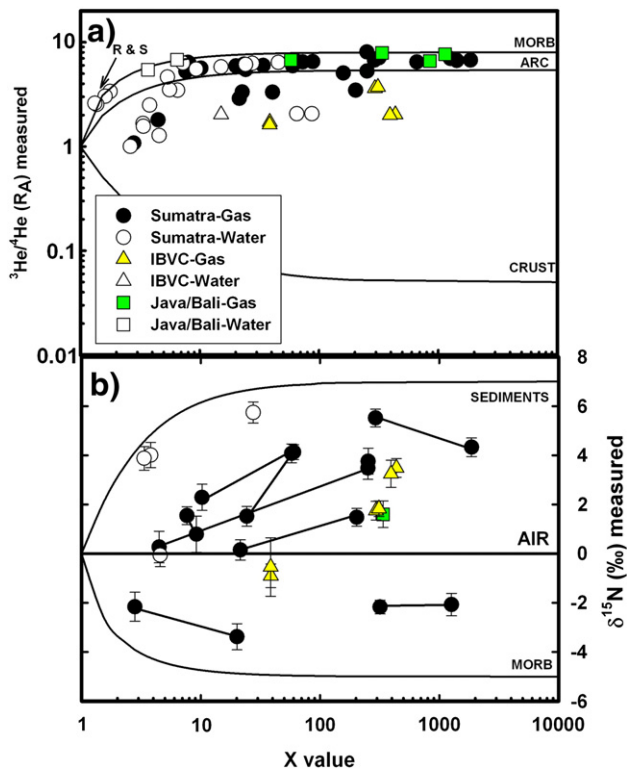


Fig. 3. a) Plot of measured He isotopes versus solubility-corrected, air-normalized He/Ne ratio (X) to assess the integrity of the He isotope results. Curves represent mixing between air-saturated water ($1 R_A$, $X = 1$) and MORB ($8 R_A$), Arc ($5.4 R_A$) and crust ($0.05 R_A$). Notably, samples with low X values (< 4) and low $^3\text{He}/^4\text{He}$ ratios are severely air-contaminated. Similarly, samples with high X values and low $^3\text{He}/^4\text{He}$ ratios are contaminated with radiogenic helium due to crustal contamination. R & S are water samples from Rajabasa and Semining. b) Plot of measured $\delta^{15}\text{N}$ versus the same X value to assess the integrity of the $\delta^{15}\text{N}$ results. Tie-lines connect samples from the same locality. Curves represent mixing between air-saturated water (0‰ $\delta^{15}\text{N}$, $X = 1$) and MORB (-5‰ $\delta^{15}\text{N}$) and sediments ($+7\text{‰}$ $\delta^{15}\text{N}$). We note that when duplicate samples from the same locality show poor agreement, the sample with the lowest X almost generally plots closer to the N isotopic composition of air (0‰).

-2.18‰) and Helatoba–Tarutung (-0.58 and -0.95‰), these are the only volcanoes to have solely negative values. We do not observe any marked difference between water and gas samples (Fig. 3). Out of four water phase samples analyzed, Dempo overlaps with the N-isotopic composition of air whereas the remaining three (Semining, Kaba and Talang) all show positive values (up to 5.92‰).

5. Discussion

5.1. Sample integrity

In this section, we adopt a step-by-step filtering protocol to test the integrity of individual samples to identify those unrepresentative of magmatic gas, due to air contamination, shallow-level crustal contamination and/or elemental fractionation within the hydrothermal systems. This approach is an essential prerequisite to revealing those samples/localities with isotopic and relative abundance He–C–N characteristics of the magma system. Only in this way is it possible to assess the relative importance of mantle source vs. crustal controls on the volatile systematics.

5.1.1. Air contamination

Atmospheric gases can act to mask and/or overwhelm the volatile characteristics of magmatic systems: this is particularly the case for He- and N-isotopes but not so for CO_2 due to the relatively low CO_2

content of air. One way to identify atmospheric contributions is to utilize sample He/Ne ratios (Fig. 3a). For example, two water phase samples from both Rajabasa and Semining have low X -values so are subject to a large air-correction to measured He isotope compositions. In addition, poor agreement between duplicate samples from these localities further suggests that one or both have experienced severe air-contamination. Generally, when duplicate samples display poor agreement for He-isotopes ($> 1 R_A$), we select the duplicate sample with the higher X value, such as in the case of samples SUM10-29 from Panururan and SUM10-25 from Bual Bauli, as being the least compromised due to air additions.

An alternative approach is to identify atmospheric contributions through the major gas chemistry. For example, N_2/Ar values lower than air (83) but higher than or equal to air-saturated water (ASW) (45) are considered to be contaminated with air and/or affected by mixing with ASW. In this respect, mixing with ASW may apply to the following: Sekincau (G-SUM10-4, 694 and 746), Sorik Marapi II (565), Semining (649), Dusan Baru (G-SUM10-5) and Pangururan (665). In addition, three samples have N_2/Ar ratios within uncertainty of ASW: gas phase samples from Rimbo Panti ($\text{N}_2/\text{Ar} \sim 32$) and Sibayak II (~ 41), and a water phase sample from Batur ($\text{N}_2/\text{Ar} \sim 38$). Furthermore, we note that a number of samples have high O_2 which also implies severe air contamination, e.g., sample 690 from Semining G-SUM-10-3 (Ratai), 674 (Marapi) and 565 (Sorik Marapi II) with O_2 content up to 27%.

The third criterion for identifying air-contaminated samples is the combination of N isotopes, overlapping with air values, and low X values (see Fig. 3b). Two samples fall under this category: Dempo (SUM10-10) and Panururan (SUM10-29).

5.1.2. Processes affecting water phase samples

5.1.2.1. Hydrothermal degassing. Phase separation processes within the hydrothermal systems have the potential to modify original magmatic values, particularly with respect to CO_2 (e.g., Ray et al., 2009). Three localities (Rajabasa, Dusan Baru, Sibayak) allow a direct comparison of He– CO_2 characteristics between gas and water phases. At each of these localities, water phase samples are characterized by higher

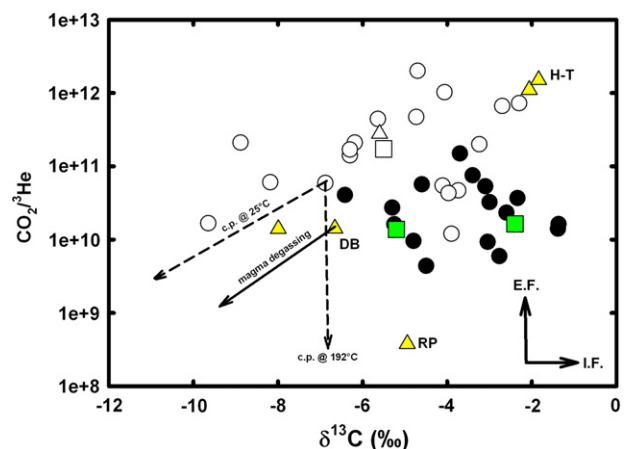


Fig. 4. Plot of $\text{CO}_2/^3\text{He}$ vs $\delta^{13}\text{C}$ for all gas and water phase samples. Trajectories show the effect of temperature dependent calcite precipitation (c. p.) at 25°C and 192°C (dashed lines) and magmatic degassing (solid line) from the water and gas phase samples which best represent the arc mantle: Kaba ($\text{CO}_2/^3\text{He} = 59.2 \times 10^9$, $\delta^{13}\text{C} = -6.9\text{‰}$) was used in the c. p. model, whereas Dusan Baru ($\text{CO}_2/^3\text{He} = 14.2 \times 10^9$, $\delta^{13}\text{C} = -6.7\text{‰}$) was used for the magma degassing model. Observations are inconsistent with both models. The effects of elemental fractionation (E.F.) of $\text{CO}_2/^3\text{He}$ ratios (vertical line) and isotope fractionation (I.F.) of $\delta^{13}\text{C}$ (horizontal line) are also shown. Note the low $\text{CO}_2/^3\text{He}$ ratio in a sample from Rimbo Panti (RP) and the high $\text{CO}_2/^3\text{He}$ ratios in samples from Helatoba–Tarutung (H–T). Dusan Baru = DB. Symbols as in Fig. 3.

$\text{CO}_2/{}^3\text{He}$ ratios, consistent with phase separation being an active process in fractionating $\text{CO}_2/{}^3\text{He}$ ratios. Because of its low solubility in aqueous fluids, helium preferentially enters the vapor phase relative to CO_2 and consequently the $\text{CO}_2/{}^3\text{He}$ ratios increases in the residual water phase (Ozima and Podosek, 2002).

Degassing of water phase samples in a hydrothermal system can be readily identified in a plot of $\text{CO}_2/{}^3\text{He}$ vs. air-corrected He concentrations (Fig. 5a). There are two notable observations: first, there is a general trend of increasing $\text{CO}_2/{}^3\text{He}$ ratios in the water samples with lower He contents. Second, independent of He content, all samples show $\text{CO}_2/{}^3\text{He}$ ratios significantly higher than the average values of arcs worldwide (GAA-global arc average) (Sano and Williams, 1996). These observations are consistent with water phase samples containing He and CO_2 which are residual following phase separation event(s).

Phase separation within a hydrothermal system can also potentially fractionate C-isotopes. We plot $\delta^{13}\text{C}$ values vs. He concentrations for all water phase samples in Fig. 5b to test for this possibility. The general negative correlation between $\delta^{13}\text{C}$ values and He concentrations is consistent with a simple model of degassing-induced isotopic fractionation of ${}^{13}\text{CO}_2$ from ${}^{12}\text{CO}_2$. Indeed, a simple model of open-degassing (Rayleigh fractionation) taking into account the solubility difference between CO_2 and He in water and the carbon isotope fractionation between gaseous CO_2 and various carbon-bearing species dissolved in the geothermal water is in good agreement with the relationship between $[\text{He}]_c$, $\text{CO}_2/{}^3\text{He}$ and $\delta^{13}\text{C}$ (Fig 5a and b).

Finally, we note that three out of the four water samples analyzed for N isotopes have relatively high $[\text{He}]_c$ concentrations ($>90 \text{ ncm}^3\text{STP/g H}_2\text{O}$) (Table 1). Although empirical evidence of N isotope fractionation is unavailable, these samples appear relatively undegassed making it unlikely that hydrothermal phase separation has affected their N-isotope values. However, one water phase sample (SUM10-10 from Dempo) has a relatively low He content ($52 \text{ ncm}^3\text{STP/g H}_2\text{O}$), a low X value, and an air-like N isotope composition: taken together, these features are consistent with hydrothermal degassing, followed by late-stage contamination by an air-like N component.

5.1.2.2. Calcite precipitation. Temperature-controlled precipitation of calcite at depth can also potentially modify $\text{CO}_2/{}^3\text{He}$ ratios and $\delta^{13}\text{C}$ values in water phase samples (Hilton et al., 1998a; van Soest et al., 1998; Ray et al., 2009). In Fig. 4, we compare the $\text{CO}_2/{}^3\text{He}$ and $\delta^{13}\text{C}$ characteristics of water and gas phase samples. We select Kaba sample SUM10-11 ($\text{CO}_2/{}^3\text{He} = 59.2 \times 10^9$, $\delta^{13}\text{C} = -6.0\text{‰}$), as an illustrative example to model this processes as it has relatively unmodified arc-like characteristics (e.g., Hilton et al., 2002). We superimpose two temperature-dependent calcite precipitation trajectories (c.p. at 25°C and 192°C) to show the potential fractionation effects associated with calcite precipitation. Notably, none of the water samples fall between the trajectories indicating they are likely unaffected by calcite precipitation. Even selecting a starting point with higher $\delta^{13}\text{C}$ (e.g., -3.9‰ e.g., Sibayak sample 667) fails to encompass the vast majority of the water samples.

5.1.2.3. Crustal contamination. Low ${}^3\text{He}/{}^4\text{He}$ ratios ($\ll 8 R_A$) accompanied by high He/Ne values could reflect a dilution of magmatic He components with crustal He in the hydrothermal system. This effect could be caused by (a) gas loss from fluids, with (residual) waters consequently more susceptible to contamination by crustal volatiles rich in ${}^4\text{He}$ (e.g., van Soest et al., 1998) and (b) significant transit distances between fluid discharge points at the surface and the point where He exsolves from a magmatic system (e.g., Sano et al., 1984).

To test for crustal contamination within the hydrothermal system, we take advantage of three localities which allow a direct comparison between He isotopes in gas and water phases. At Rajabasa, a gas phase He isotope value of $8.1 R_A$ is higher than that measured in water samples (3.0 to $5.5 R_A$), consistent with preferential addition

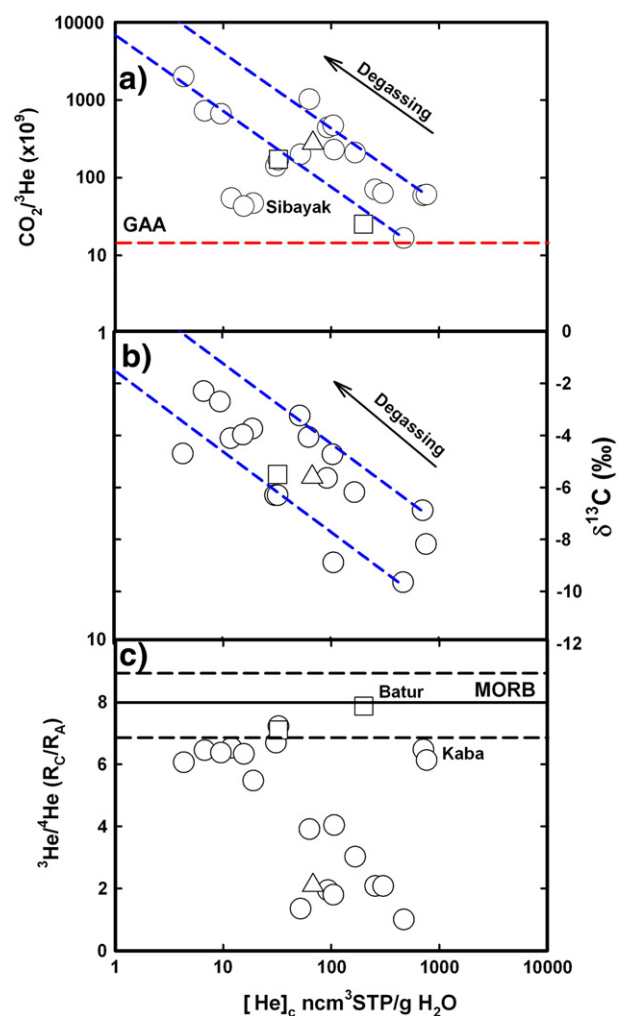


Fig. 5. a) Plot of $\text{CO}_2/{}^3\text{He}$ vs. air-corrected He concentrations for water samples only. Except for 3 samples from Sibayak volcano, there is a general trend of decreasing helium concentration in the water phase with higher $\text{CO}_2/{}^3\text{He}$ ratios. The global arc average (GAA—red dashed line) is from Sano and Williams (1996). b) Plot of $\delta^{13}\text{C}$ values vs. He concentrations for water samples only. The negative correlation is consistent with degassing-induced isotopic fractionation of carbon. c) Plot of He isotopes vs. He concentrations for all water samples. Except for a few samples (e.g., Kaba and Batur) there is a general negative correlation consistent with addition of radiogenic (crustal) He to water phase samples. The range for MORB of $8 \pm 1 R_A$ is from Graham (2002). Trajectories for open-degassing are shown as blue dashed curves in panels a and b. The model on panel a uses the equation: $(\text{CO}_2/\text{He})_{\text{final}} = (\text{CO}_2/\text{He})_{\text{initial}} \times f^{(\alpha-1)}$ where f is the fraction of He remaining after degassing and α is the fractionation factor calculated at $71.4^\circ\text{C} = 3.00 \times 10^{-2}$ (following Weis, 1971,1974 and de Leeuw et al. 2010). Similarly, the model in Fig. 5b was constructed using the equation: $\delta^{13}\text{C}_{\text{res}} = [(1/\alpha) \times (\delta^{13}\text{C}_{\text{ini}} + 1000) \times f^{(1/\alpha-1)}] - 1000$ where f is the fraction of He remaining after degassing and α is the isotopic fractionation factor between aqueous bicarbonate and gaseous CO_2 calculated at $95^\circ\text{C} = 1.347$ (following Szaran, 1997). Two samples from Kaba (SUM10-12) and Dempo (SUM10-14) with the highest $[\text{He}]_c$ are used as starting points for the degassing trends. For model details see de Leeuw et al. (2010). Symbols as in Fig. 3.

of radiogenic He to the water phase. However, the case is more equivocal for both Dusan Baru hydrothermal site, where He isotopes show excellent agreement between the two phases, and Sibayak volcano where summit samples show consistent values of $6.7 R_A$, overlapping with water phase samples (5.5 and $7.2 R_A$) located on the flanks.

In Fig. 5c, we plot He isotopes vs. He concentration for all water samples to assess the general effects of crustal contamination. In this respect, we assume that He addition increases as a function of water-rock interaction within the hydrothermal reservoir such that it represents a proxy for distance traveled from the point of

exsolution from the magmatic system. Except for two samples from Kaba volcano and one sample from Batur, there is a significant negative correlation consistent with addition of radiogenic (crustal) He to water phase samples. Thus, the crustal contaminant must have relatively high helium concentrations and a low $^3\text{He}/^4\text{He}$ ratio. Moreover, by comparing Fig. 5b and c, we note that samples with radiogenic crustal addition displays the lowest $\delta^{13}\text{C}$ values, indicating that the contaminant is likely to either contain carbon of organic derivation or has fractionated $\delta^{13}\text{C}$ values. As discussed in Section 5.1.2.1 and illustrated in Fig. 5b, it is the high $\delta^{13}\text{C}$ values (low [He]) which are consistent with degassing-induced $\delta^{13}\text{C}$ fractionation. Therefore, unless the starting $\delta^{13}\text{C}$ values are unusually low (i.e., magmas are characterized by organic C-like values) then the former explanation is preferred. In the case of water phase samples from Semining (3.0 R_A) and Talang (2.0 R_A), they also possess N isotope compositions ($\delta^{15}\text{N}_C$) typical of sediments, at 5.08 and 5.11‰, respectively. For these samples, therefore, the origin of the nitrogen is likely to be shallow levels in the crust (Inguaggiato et al., 2004). Although somewhat more equivocal, we note that the most positive $\delta^{15}\text{N}_C$ value in the dataset (Kaba at 5.92‰), is characterized by both high He concentrations (713 ncm³/g H₂O) and mantle-like He-isotopes (6.5 R_A) and $\delta^{13}\text{C}$ values (−6.9‰). In this case, it is unlikely that N is derived from shallow organic material.

5.1.3. Processes affecting gas phase samples

5.1.3.1. Magma degassing. Magma degassing will affect not only the elemental abundance of magmatic volatiles, as a function of their different solubilities in melt, but also the isotopic composition of specific volatiles such as CO₂ (e.g., Holloway and Blank, 1994). Degassing of magmatic volatiles will not only lower the CO₂/³He ratio due to the preferential loss of CO₂ relative to He, (e.g., Hilton et al., 1998b), but also the $\delta^{13}\text{C}$ value. Assuming an isotopic fractionation factor of 2‰ between ¹³CO₂ in the gas phase and ¹³CO₂ remaining in the melt (Mattey, 1991), volatiles residual after degassing will be depleted (i.e., evolve to lower $\delta^{13}\text{C}$ values) as degassing progresses. Notably, style of degassing (open vs. closed system) will not affect the general fractionation trends, i.e., CO₂/³He ratios and $\delta^{13}\text{C}$ values will always decrease in the melt, but it will affect the magnitude of any fractionation.

If we select Dusan Baru (SUM10–13) with a $\delta^{13}\text{C}$ value (−6.7‰) representative of the mantle wedge (cf. Sano and Marty, 1995), it is clearly seen that no samples fall along the magma degassing trajectory (Fig. 4). Even if we were to choose a different end-member composition with a more positive $\delta^{13}\text{C}$ value (e.g., from −6.7‰ to −4.6‰), magma degassing still fails to account for the $\delta^{13}\text{C}$ data. Magma degassing can also be disregarded as a viable means to explain the low CO₂/³He ratio from the Rimbo Panti acid spring as its starting compositions can be considered inappropriate for the arc mantle (i.e., very low CO₂/³He ratio of 0.38 × 10⁹).

With respect to nitrogen, there is no consensus on degassing-induced isotopic fractionation of nitrogen (see contrasting views in the discussions of Cartigny and Ader, 2003 and Marty and Dauphas, 2003b). Indeed, evidence has been presented against N isotope fractionation during magma degassing based on a study of olivine and geothermal gases collected at the same locations (Fischer et al., 2005). This study shows similar $\delta^{15}\text{N}$ values for both types of sampling media.

5.1.3.2. Crustal contamination. The majority of water phase samples have been modified by crustal contamination (Section 5.1.2.3), and the same phenomenon could potentially affect gas phase samples. For example, two gas phase samples from IBVC, i.e., Rimbo Panti (0.38 × 10⁹) and Helatoba–Tarutung (> 1000 × 10⁹), fall outside the range of CO₂/³He ratios typical of all other gas samples (~50 × 10⁹ to ~1 × 10¹¹). Also, samples from Dusan Baru have the lowest $\delta^{13}\text{C}$ values (−6.7 and −8.0‰) among the gas phase samples.

Significantly, all three localities are located a considerable distance from volcanic summits and have large relative contributions of radiogenic helium (³He/⁴He between 1.7 R_A and 3.7 R_A). In addition, samples from Rimbo Panti and Dusan Baru have high CH₄ contents (5 and 7 %). Assuming that such high methane concentrations can only be produced by inputs of thermogenically-produced CH₄ from crustal sediments (Taran, et al., 1998), these observations are consistent with these samples having experienced significant crustal contamination. Other likely processes affecting the IBVC samples include: 1) input of CO₂ from the crust, from decarbonation reactions, which may well explain the high CO₂/³He ratios (> 1000 × 10⁹) in samples from Helatoba–Tarutung; and 2) loss of CO₂, presumably by means of carbonate and/or calcite precipitation, which would then produce anomalously low CO₂/³He ratios as observed at Rimbo Panti.

From a helium isotope perspective, the IBVC samples are the most crustally-contaminated gas samples in the study. In this respect, we might expect a negative relationship between He and N isotopes—assuming that crustal contamination is fingerprinted by high $\delta^{15}\text{N}$ (e.g., Inguaggiato et al., 2004). However, no such relationship is evident (e.g., Helatoba–Tarutung has $\delta^{15}\text{N} < 0$) suggesting an important role for mixing with mantle N components and a muted crustal N input at this locality. Alternatively, mixing with secondary N in a moderate- to low-temperature hydrothermal system at shallow levels of the crust may explain the negative $\delta^{15}\text{N}$ values from Helatoba–Tarutung (see Li et al., 2009).

5.1.4. Spatial controls on volatile integrity: flank vs. summit variations

Proximity of sampling sites to volcanic centers or summits is often a primary criterion for sampling pristine magmatic gas, with low He isotope ratios frequently observed at more distal discharge vents (e.g., Sano et al., 1984; Marty et al., 1989; van Soest et al., 1998; Barry et al., 2013–this issue). Three volcanoes in Sumatra allow us to consider this issue: Sorik Marapi, Rajabasa and Sibayak. In the case of two flank localities from Sorik Marapi volcano, sampled only a few km apart, they show contrasting helium isotope ratios in the same sample medium (gas), ~3 R_A (n=4) vs. 6 R_A (n=3). Such a large difference in ³He/⁴He probably indicates increasing (and heterogeneous) additions of crustal He with distance from the central conduit of the volcano. Different samples on the flanks of Rajabasa volcano (n=5) vary from 3.0 R_A to 8.1 R_A , with the highest helium isotope ratios (and most MORB-like ratios of CO₂/³He) found in a single gas sample from an acid spring (free gas phase)—all other samples showing lower ³He/⁴He ratios are (spring) water phase samples. In contrast, flank samples (n=4) at Sibayak volcano agree well with summit samples (n=3) in their He isotopes (and carbon abundance and isotope characteristics). Therefore, if this ‘distance’ effect is to be recognized for gas samples, it has to be taken on a case-by-case basis, with volcanoes with many sampling locations (summit and flank) likely to yield more definitive conclusions. However, for Sorik Marapi and Sibayak, we deem the highest values at both these volcanoes as most representative of the magmatic source with lower values reflecting crustal additions of radiogenic He associated with the hydrothermal system.

5.1.5. Possible temporal variations

Nine volcanic centers and one IBVC locality were sampled in 1991 and 2010, thus enabling combination of the two datasets for assessment of temporal changes. However, there is some uncertainty regarding the exact locations of sampling. Even with this caveat, good agreement (<1 R_A) is found at Sekincau, Dempo, Marapi, Sorik Marapi, Bual Buali, Panururan, Sibayak and Dusan Baru whereas poorer agreement (>2 R_A) characterizes Rajabasa and Semining. These observations suggest that there has been limited temporal variation in chemical and isotopic composition of emitted gases and fluids over the two-decade hiatus between sampling expeditions. For the most part, differences between the two datasets can be

explained by varying degrees of air addition, e.g., samples from the flanks of Seminung and Dempo. When samples of the same medium contain very small contributions of air, i.e., have large X values, $^3\text{He}/^4\text{He}$ ratios are in excellent agreement—e.g., Sibayak has a $^3\text{He}/^4\text{He}$ ratios of $6.7 R_A$ (1991) and $6.7\text{--}6.8 R_A$ (2010).

Interestingly, four summit samples from Marapi, Sumatra's most active volcano, vary beyond analytical uncertainty ($<0.2 R_A$) from $\sim 6.4 R_A$ in 1991 to $\sim 7.0 R_A$ in 2010. GPS coordinates are unavailable from the first sampling expedition so it is impossible to determine if samples were from the same fumarole fields. However, it is possible that an increase in helium isotope ratios accompanied a magma re-charging event at the volcano prior to the renewed activity in 2011 (Smithsonian Institution, 2011).

5.1.6. Summary

In summary, in identifying samples which are likely representative of the magmatic systems of the western Sunda arc, we have confidence in data integrity of samples with a) X values greater than ~ 3 , b) samples which show good agreement between duplicates, and c) samples which show significant deviations from the N isotopic composition of air combined with relatively high X values. A total of 7 samples have experienced sufficient modification by air-contamination that they are unlikely to reflect primary magma characteristics: 681 and 726 (Rajabasa); 690 and 649 (Seminung); SUM10-14 (Dempo); SUM10-25 (Bual Buali); and SUM10-29 (Panururan). However, despite low X values, duplicate samples from Rajabasa (681 and 726) and Seminung (690 and 649) show good agreement after air-correction. Thus, even if water phase samples have been masked by air contamination, they may still preserve $^3\text{He}/^4\text{He}$ ratios (after correction) that approach primary magma characteristics. However, the majority of water phase samples have been affected by phase separation within the hydrothermal system and their $\delta^{13}\text{C}$ and $\text{CO}_2/^3\text{He}$ values are likely unrepresentative of the magmatic source. In addition, a number of samples located at a considerable distance from the volcanic centers (i.e., all the IBVC localities: Dusan Baru, Rimbo Pantu and Helatoba–Tarutung) and/or at volcanic flank localities (i.e., Rajabasa, Seminung, Dempo, Talang and Sorik Marapi) have experienced significant crustal contamination in the hydrothermal system thus rendering them inappropriate for deducing magmatic sources. Crustal contamination may possibly affect carbon characteristics of gas samples but the effect becomes clear only at low $^3\text{He}/^4\text{He}$ ratios (i.e., samples from the IBVC localities). In turn, the IBVC samples and water phase flank samples could be important for discerning the likely volatile composition of crustal material in Sumatra.

5.2. The western Sunda arc—along-strike variations

5.2.1. $^3\text{He}/^4\text{He}$ ratios

In Fig. 6a, we plot the highest $^3\text{He}/^4\text{He}$ ratio found in water and gas samples from each sample location (summit and flank locations) as a function of latitude. The majority of fluid samples (gas and water) from the western Sunda arc have air-corrected $^3\text{He}/^4\text{He}$ ratios in the range of 5.1 to $8.1 R_A$, typical of arcs worldwide (Hilton et al., 2002). Significantly, additions of radiogenic helium are found in flank water phase samples from Rajabasa, Seminung, Dempo, and Talang, and also in gas phase samples from Sorik Marapi. Additionally, fluids associated with major fault systems lying in between volcanic centers (IBVC), i.e., Dusan Baru, Rimbo Pantu and Helatoba–Tarutung, i.e., all have significant radiogenic additions.

In Fig. 6b, we plot only the highest $^3\text{He}/^4\text{He}$ ratio for an individual volcano, and thus the most likely representative value of magma source characteristics. Additions of radiogenic He are still evident among five samples (Talang, Dempo and three IBVC localities) in this filtered dataset. It is important to note that these two volcanic centers are characterized on the basis of a single collection site only, so we cannot rule out the presence of a higher He isotope ratio at

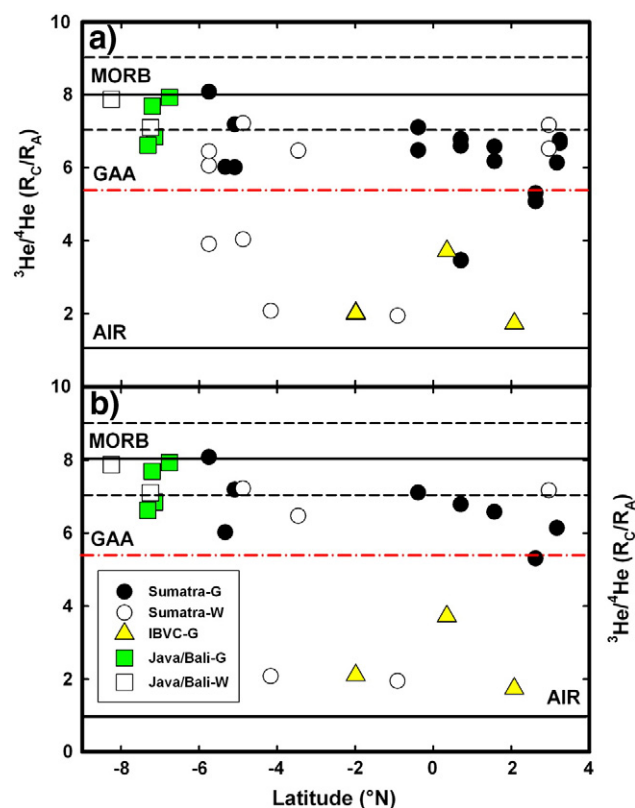


Fig. 6. a) Profile of air-corrected He isotopes vs. latitude for the western Sunda gas and water samples. The highest $^3\text{He}/^4\text{He}$ ratio found in water and gas samples from each location (flank and summit) is plotted. b) Filtered version of the same dataset as in a) but with only the single highest $^3\text{He}/^4\text{He}$ ratio for any given volcano plotted. Notably, only water phase samples from Dempo and Talang and samples from the IBVC show significant additions of radiogenic helium. The range for MORB of $8 \pm 1 R_A$ is from Graham (2002) and the global arc average (GAA) of $5.4 R_A$ from Hilton et al. (2002).

these volcanoes, especially since no summit fumaroles were sampled. Beyond these excursions, there is no apparent N–S control on $^3\text{He}/^4\text{He}$ ratios. Interestingly, our Java and Bali samples show very little evidence for significant radiogenic additions and span a rather limited range of 6.6 to $7.9 R_A$ but these observations are based on a smaller sample set.

5.2.2. $\delta^{13}\text{C}$ (CO_2) values and $\text{CO}_2/^3\text{He}$ ratios

In Fig. 7a, we plot $\delta^{13}\text{C}$ values as a function of latitude for the same samples plotted in Fig. 6a (i.e., summit and flank gas locations but excluding all water phase samples). In contrast to helium isotopes, carbon isotopes tend to show the highest values in the south and north of the western Sunda arc. Significantly, greater heterogeneity is evident from the northern sector of the arc, where the highest values are observed (up to -1.4%), compared to other sections. Java and Bali samples and samples from IBVC also have high $\delta^{13}\text{C}$, i.e., they overlap with other samples of Sumatra.

In Fig. 7b, we plot $\text{CO}_2/^3\text{He}$ ratios as a function of latitude for the same samples as in Fig. 7a. Except for one sample (Rimbo Pantu), $\text{CO}_2/^3\text{He}$ ratios along the west Sunda arc are always higher than the ratios observed in MORB ($\sim 1.5 \times 10^9$; Marty and Jambon, 1987). In fact, of the entire dataset ($n=24$), only eight samples plot below the GAA ($\sim 1.6 \times 10^{10}$; Sano and Williams, 1996). When considering gas phase samples from the volcanic centers only (i.e., excluding the IBVC samples), $\text{CO}_2/^3\text{He}$ ratios increase from south to north along the Sumatran transect, where ratios significantly higher than the GAA become generally more prevalent north of 1°S . Notable

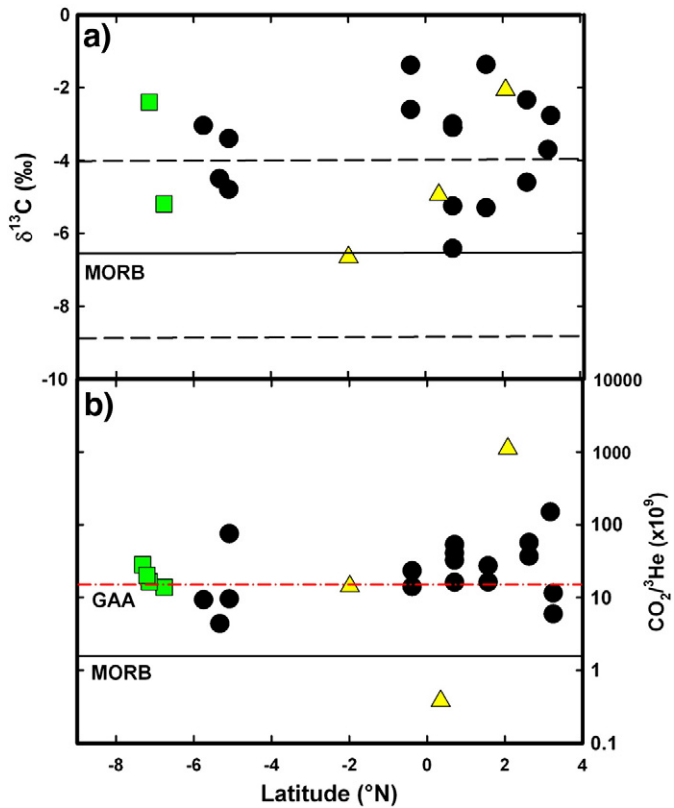


Fig. 7. Along-arc variations in a) $\delta^{13}\text{C}$ and b) $\text{CO}_2/{}^3\text{He}$ for geothermal gases from the western Sunda arc. Note that only $\delta^{13}\text{C}$ values and $\text{CO}_2/{}^3\text{He}$ ratios with the highest ${}^3\text{He}/{}^4\text{He}$ ratio at any given location is plotted (i.e., Fig. 6a). Dashed and solid horizontal lines show the MORB range of $\delta^{13}\text{C}$ values: -6.5 ± 2.5 (Sano and Marty, 1995), $\text{CO}_2/{}^3\text{He}$ range for arcs worldwide (GAA) of 1.6×10^{10} (Sano and Williams, 1996) and the MORB range of 1.5×10^9 (Marty and Jambon, 1987). Symbols as in Fig. 3.

exceptions to this trend are two summit samples ($\sim 6 \times 10^9$) from Sibayak and flank samples ($\sim 70 \times 10^9$) from Sekincau. Samples from Java and Bali either overlap with GAA or have slightly higher ratios.

5.2.3. N_2/He and N_2/Ar ratios and $\delta^{15}\text{N}$ (N_2) values

In Fig. 8a–c, we plot the N_2 characteristics (N_2/Ar and N_2/He and $\delta^{15}\text{N}_\text{C}$) as a function of latitude. Note that for $\delta^{15}\text{N}_\text{C}$ we plot the same samples as in Fig. 6a as we have no evidence of sampling bias (Sections 5.1.2 and 5.1.3). Over the whole Java–Bali–Sumatra transect N_2/Ar , N_2/He and $\delta^{15}\text{N}_\text{C}$, vary from ~ 40 to $\sim 17,000$, ~ 40 to $\sim 2 \times 10^5$, and -3.91 to $+5.92\%$, respectively, consistent with the range found previously in arc-related volcanoes (e.g. Fischer et al., 2002; Elkins et al., 2006; Mitchell et al., 2010). The data, therefore, fall within reported ranges of possible sources contributing to the nitrogen inventory of gases in volcanic arcs, i.e., from typical mantle values (i.e., Marty and Dauphas, 2003a) to values significantly higher, akin to those found in oceanic sediments (see Peters et al., 1978; Fischer et al., 2002). These high ratios, as well as positive $\delta^{15}\text{N}_\text{C}$, are often attributed to a large contribution from degrading organic-rich oceanic sediments on the down-going slab (Fischer et al., 2002; Taran and Giggenbach, 2003). No systematic changes are observed in the N_2/Ar and N_2/He ratios and $\delta^{15}\text{N}_\text{C}$ systematics along the strike of the arc but in agreement with observations for $\delta^{13}\text{C}$ values, both higher and lower N_2/Ar ratios and $\delta^{15}\text{N}_\text{C}$ values are observed in the southern and northern segments of the arc. The data from the Java and the Bali segments fall within the Sumatra range.

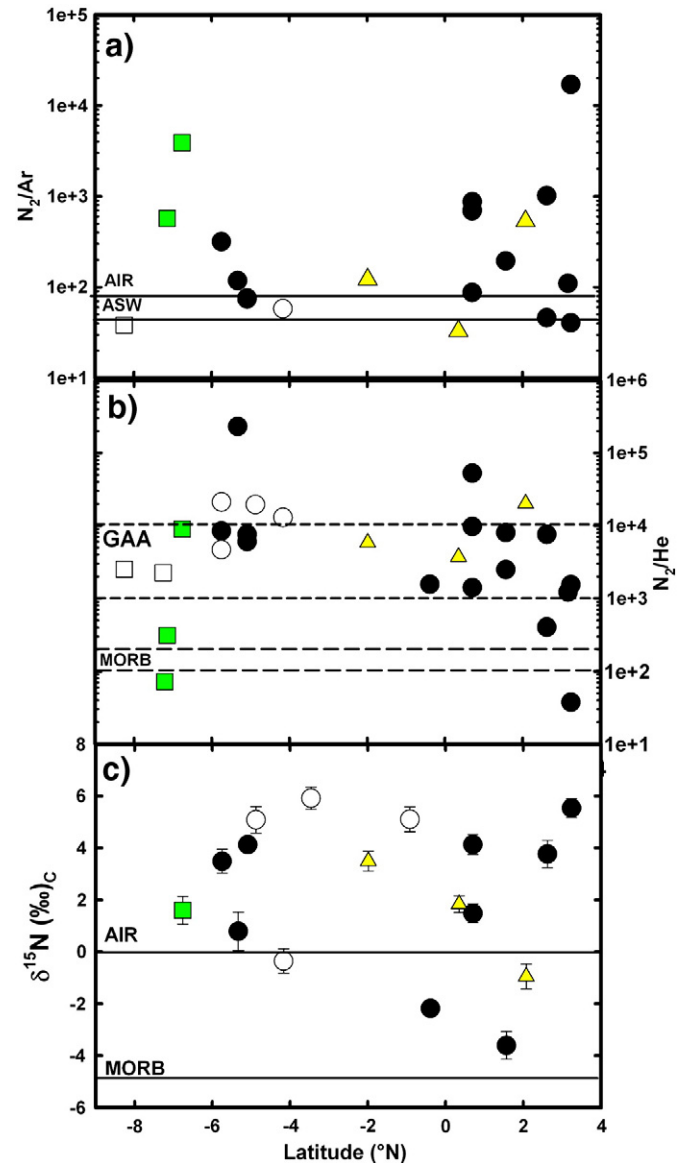


Fig. 8. Profiles of a) N_2/Ar , b) N_2/He and c) $\delta^{15}\text{N}_\text{C}$ vs. latitude for geothermal gases and fluids from the western Sunda arc. Only $\delta^{15}\text{N}_\text{C}$ values with the highest ${}^3\text{He}/{}^4\text{He}$ ratio at any given location are plotted. The solid horizontal lines in a) shows ratios for air (83.5) and air-saturated water (ASW) (45). Dashed, horizontal lines in b) represents the GAA and MORB N_2/He range (based on Mitchell et al., 2010). The MORB range in c) is from Marty and Dauphas, 2003a. Symbols as in Fig. 3.

5.3. Major gas provenance along the western Sunda arc segment

The majority of gas samples have CO_2 and N_2 systematics which are likely to give insight into magmatic source characteristics along the western Sunda arc segment. In this section, we assess the provenance of the magmatic CO_2 and N_2 and discuss inter-relationships between these two major gas phases.

5.3.1. CO_2 provenance

We plot $\text{CO}_2/{}^3\text{He}$ vs. $\delta^{13}\text{C}$ for all filtered samples (Section 5.1.4) together with possible contributory end-member compositions for MORB-mantle (M), marine carbonate component (limestone) (L) and a sedimentary (S) organic carbon (Fig. 9) (Sano and Marty, 1995). Another potentially important C reservoir in subduction environments is the altered oceanic crust (AOC). We note that Shilobreeva et al. (2011) recently estimated a $\delta^{13}\text{C}$ value of -4.7% as representative of

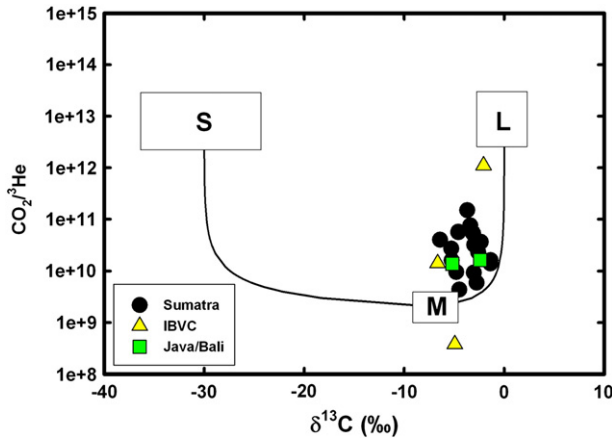


Fig. 9. Plot of $\text{CO}_2/{}^3\text{He}$ vs $\delta^{13}\text{C}$ for western Sunda arc samples. Superimposed are end-member compositions of a sedimentary-derived carbon source (S), calcareous- or limestone-derived source (L), and mantle-derived (M) following Sano and Marty (1995). Simple binary mixing between mantle and carbonate components cannot explain the data, and up to a 25% contribution from a sedimentary source, hosting organic carbon, is required.

average altered oceanic crust (AOC) which makes it indistinguishable from mantle wedge carbon. This observation, together with arguments by de Leeuw et al. (2007) that it is unlikely the AOC contributes C to the arc inventory, at least in the case of Central America, allows us to discount AOC in the following approach. As L, S and M end-members have distinctive $\text{CO}_2/{}^3\text{He}$ and $\delta^{13}\text{C}$ ratios (M: 1.5×10^9 ; -6.5% ; L: 1×10^{13} ; 0% ; S: 1×10^{13} ; -25%), it allows determination of CO_2 provenance along the western Sunda arc (Table 3). From Fig. 9 it is apparent that the CO_2 is dominated by mixing between M and L components; however, the carbon characteristics of the samples are inconsistent with simple binary mixing between these two end-members, and require up to a 25% contribution from an organic sedimentary carbon component.

As discussed (Section 5.2.2), higher and more variable $\text{CO}_2/{}^3\text{He}$ ratios and generally higher $\delta^{13}\text{C}$ values, are observed along the arc towards the north (Fig. 7). This observation can be investigated more closely by comparing the relative contribution of L, M, and S along the strike of the arc. In Fig. 10a, we plot the ratio of CO_2 derived from the two sedimentary components (L + S) relative to that from the mantle component (M) for the same samples as in Fig. 6b, and we note that this ratio increases northward along the arc. If variations to the (L + S)/M ratio are related to the subducted sediments alone, then this observation suggests fundamental changes in the subducting Himalayan sedimentary carbon budget of the down-going Indo-Australian Plate offshore Sumatra. However, if the overlying crust has an impact on this relationship then there are fundamental differences between the Sundaland basement in northern Sumatra and south Sumatra/Java/Bali. This point is discussed in Section 5.4.

5.3.2. N_2 provenance

In a manner analogous to CO_2 , the air-corrected (magmatic) N_2 signal is resolved into its various source components using a simple mixing model. Potential sources of nitrogen include the mantle wedge, subducted hemipelagic sediments, shallow crustal sediments, and possibly deep crustal rocks and AOC (e.g., Mitchell et al., 2010). In contrast to organic seafloor sediments with $\delta^{15}\text{N}$ values from $+5$ to $+7\%$ (Sadofsky and Bebout, 2004; Li and Bebout, 2005), the Earth's upper mantle is characterized by a distinct isotopic composition, estimated at -5% (Marty and Dauphas, 2003a). Again, there is considerable overlap between mantle $\delta^{15}\text{N}$ values and AOC ($\delta^{15}\text{N}$ of -5.2% ; Li et al., 2007) which precludes resolution between these potential sources. As an initial approach, however, we calculate the fraction of sediment-

Table 3

Quantitative estimates of the relative contribution (%) of mantle (M), limestone (L) and sedimentary (S) sources to western Sunda samples.

Location	Sample ID	Carbon source ^a			(L+S)/M ^b	S/M ^b	Nitrogen source ^c		
		M	L	S			M	S	S/M ^b
<i>Sumatra–volcanoes</i>									
Rajabasa	SUM10-2	10.7	81.5	7.8	8.3	0.7	29.3	70.8	2.4
Ratai (Hulubelu)	SUM10-4	19.9	72.2	7.9			44.8	55.3	
	SUM10-6	22.8	67.1	10.1	3.4	0.4	52.0	48.0	0.9
	SUM10-7	11.1	77.2	11.7			45.5	54.4	
Sekincau	694	1.3	87.6	11.0					
	746	1.4	87.6	11.0					
	SUM10-18	8.8	84.5	6.7			75.6	24.4	
	SUM10-20	7.1	89.8	3.1	13.1	0.4	75.6	24.4	0.3
Marapi	674	4.4	88.5	7.0					
	680	4.3	88.0	7.7					
	SUM10-22	2.6	80.2	17.2			38.1	61.9	
	SUM10-23	2.5	76.7	20.9	39.8	8.5	23.9	76.1	3.2
Sorik Marapi	SUM10-27	6.2	77.7	16.2			46.0	54.0	
	Cu-tube-2	3.7	84.3	12.0			57.4	42.6	
	701	3.1	87.6	9.3					
	741	1.9	88.2	9.9					
Bual Buali	SUM10-24	6.1	90.6	3.2			88.4	11.6	0.1
	SUM10-25	1.6	89.4	9.0			90.9	9.1	
	675	3.7	79.5	16.9	26.4	4.6			
Panururan	SUM10-29	4.6	91.0	4.3			57.8	42.2	
	SUM10-30	2.7	90.1	7.2	36.0	2.7	26.9	73.1	2.7
	665	1.8	83.3	15.0					
Singabung	734	0.7	87.2	12.2	150.8	18.5			
Sibayak	SUM10-26	17.4	73.7	8.9			22.3	77.8	
	SUM10-28	16.8	77.6	5.6	3.0	0.3	12.2	87.8	7.2
<i>Sumatra–IBVC</i>									
Dusan Baru	SUM10-13	7.0	72.3	20.7	13.2	2.9	29.2	70.8	2.4
	SUM10-16	7.1	67.8	25.1			31.2	68.8	
Rimbo Panti	SUM10-19						43.8	56.3	
	SUM10-21						43.1	56.9	1.3
Helatoba T.	Cu-tube-3	0.1	93.1	6.8			66.3	33.8	0.5
	Cu-tube-4	0.1	93.8	6.1			63.2	36.8	
<i>Java–volcanoes</i>									
Tangkuban P.	SUM10-1	7.2	77.0	15.8	12.8	2.2	45.0	55.0	1.2
Guntur	721	6.1	87.2	6.7	15.4	1.1			

^a Calculated according to $(^{13}\text{C}/^{12}\text{C})_{\text{obs}} = M(^{13}\text{C}/^{12}\text{C})_{\text{M}} + L(^{13}\text{C}/^{12}\text{C})_{\text{L}} + S(^{13}\text{C}/^{12}\text{C})_{\text{S}}$, $1/(\text{CO}_2/{}^3\text{He})_{\text{obs}} = M/(\text{CO}_2/{}^3\text{He})_{\text{M}} + L/(\text{CO}_2/{}^3\text{He})_{\text{L}} + S/(\text{CO}_2/{}^3\text{He})_{\text{S}}$, and $M + L + S = 1$ and with end-members from Sano and Marty (1995).

^b Ratio is only calculated for the sample with highest $R_{\text{C}}/R_{\text{A}}$ (see Table 1 and Fig. 6b).

^c Calculated according to $\delta^{15}\text{N}_{\text{c}} = f_{\text{sed}} \times \delta^{15}\text{N}_{\text{sed}} + (1 - f_{\text{sed}}) \times \delta^{15}\text{N}_{\text{man}}$ and $f_{\text{man}} + f_{\text{sed}} = 1$ with end-member compositions from Fischer et al. (2002).

derived and mantle-derived nitrogen in a binary sediment-mantle mixture using the air-corrected $\delta^{15}\text{N}_{\text{c}}$ values ($\delta^{15}\text{N}_{\text{c}}$) using the following isotope mass balance equations:

$$\delta^{15}\text{N}_{\text{c}} = f_{\text{sed}} \times \delta^{15}\text{N}_{\text{sed}} + (1 - f_{\text{sed}}) \times \delta^{15}\text{N}_{\text{man}} \quad (1)$$

$$f_{\text{man}} + f_{\text{sed}} = 1 \quad (2)$$

where $\delta^{15}\text{N}_{\text{c}}$ is the air-corrected $\delta^{15}\text{N}_{\text{c}}$ composition of the samples, $\delta^{15}\text{N}_{\text{sed}} = +7\%$, $\delta^{15}\text{N}_{\text{man}} = -5\%$, and f_{sed} and f_{man} are the fractions of sediment-derived and mantle-derived nitrogen, respectively. The calculated fractions are given in Table 3 together with the ratio of sedimentary to mantle (S/M) nitrogen for samples with the highest ${}^3\text{He}/{}^4\text{He}$ ratios from each volcano (Fig. 6b). In Fig. 10b, we plot the S/M ratio as

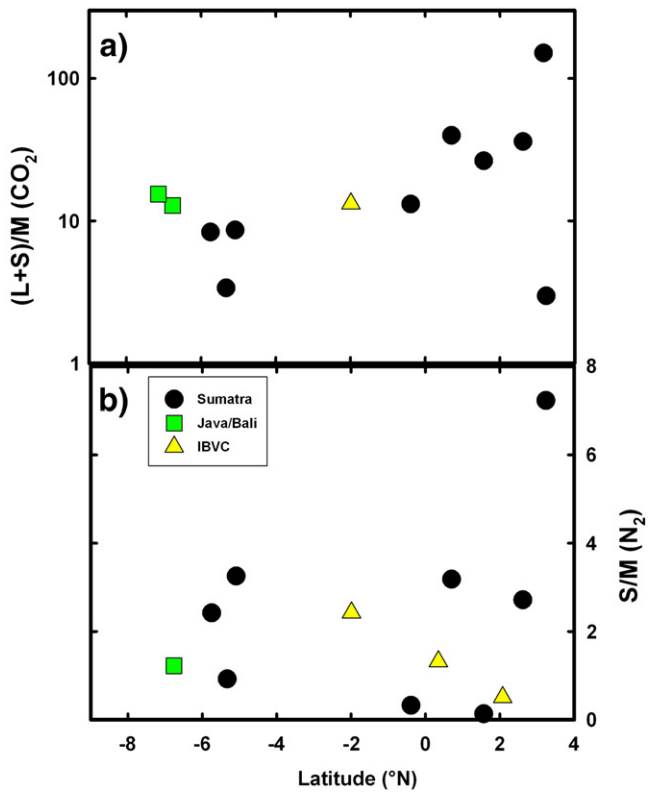


Fig. 10. a) Plot of $(L+S)/M$ (CO_2) as a function of latitude. Preferential contribution from the two sedimentary components (L+S) over the mantle component (M) is evident from south to the north. b) Plot of S/M (N_2) as a function of latitude. No apparent latitudinal changes are observed although we note the high L/M ratio (~ 7) at Sibayak.

a function of latitude. We note that in contrast to results from carbon, there are no major spatial (i.e., latitudinal) changes in the N_2 provenance characteristics along the N-S profile of the western Sunda arc. However, we note that samples from Sibayak have the highest S/M ratios of ~ 7 . We infer that the sedimentary nitrogen contribution is mostly consistent along the strike of the arc although the highest value occurs in the northernmost regions. This observation is consistent with the (sedimentary) origin of CO_2 which also appears enhanced in northern Sumatra (Section 5.3.1 and Fig. 10a).

5.3.3. Co-variations of He, C and N isotopes

The first-order observation of C and N isotope variations along the western Sunda arc suggests that marine carbonate and organic sedimentary material are the dominant contributors of CO_2 and N_2 to the volatile budget, respectively. In Fig. 11a, we plot $\delta^{13}\text{C}$ (CO_2) versus $\delta^{15}\text{N}_c$ (N_2) for all gas samples from each location containing the highest $^3\text{He}/^4\text{He}$ together with end-member components M (MORB mantle), M-L (MORB-carbonate hybrid) and S (sediments) (Sano and Marty, 1995; Marty and Dauphas, 2003a; Li and Bebout, 2005). The IBVC samples (triangles) are plotted for comparison. A model of binary mixing between a C-fluxed (M-L hybrid) MORB mantle wedge and carbonate sediments, readily explains these relationships (Fig. 11a). The relative C/N ratios between sedimentary and mantle wedge components is expressed as K-values (where $K = (C/N)_S / (C/N)_M$). K values are $\ll 1$ and range from 0.025 to 0.25, indicating that the sedimentary end-member is characterized by a marked enrichment in its N/C ratio relative to a MORB-carbonate mixture (i.e., M-L). This observation is consistent with calculated S/M ratios in Table 3. Conversely, the

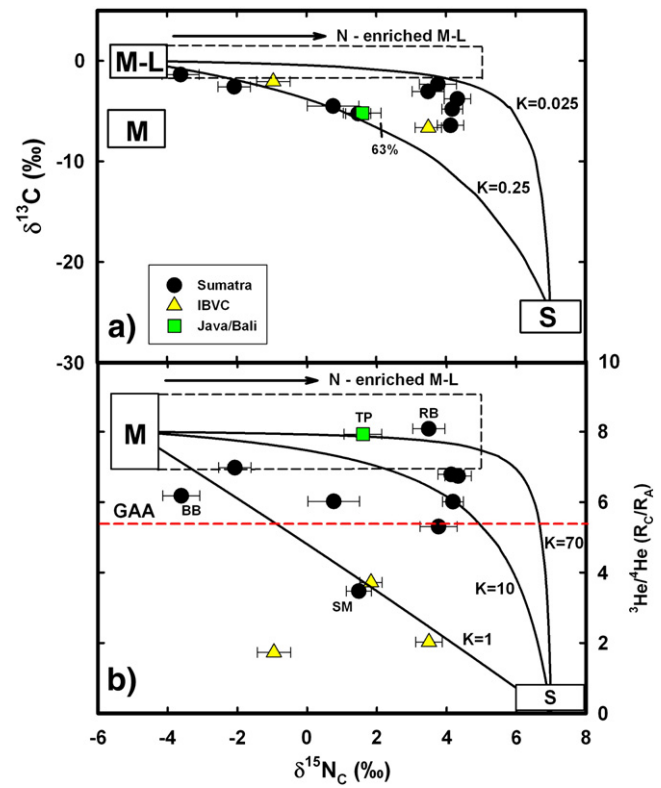


Fig. 11. a) Plot of carbon and nitrogen isotopes ($\delta^{15}\text{N}$ -corrected for air) in geothermal gases from the western Sunda arc. Binary mixing between a MORB-carbonate mixture (M-L) and a sedimentary component (S) with organically-derived carbon and nitrogen explains the data. Significantly, a component that hosts unmodified mantle wedge volatiles (M) is not likely to play a role, at least not in controlling the carbon characteristics. K mixing values between 0.025 and 0.25 demonstrate significant heterogeneity in the N/C ratio in one or both end-members. Tick indicates 63% mantle-carbonate (M-L) contribution. Dashed horizontal box indicates the possible composition of an N-enriched M-L end-member. b) Plot of helium and nitrogen isotopes (both corrected for air) for the same samples as in a). By adopting a value of $5.4 R_A$ as the lower limit for the mantle wedge He, a simple binary mixing between the mantle wedge and subducted sediments can explain most of the data. Samples from the volcanic centers can be explained by K values between 1 and 70, and demonstrate large enrichment of the sediment N_2/He ratios, relative to those of the mantle, which is consistent with fluids being dominated by MORB helium and subducted sedimentary nitrogen. Significantly lower K values (≤ 1) are needed to explain all other samples. Dashed horizontal box indicates the possible composition of a N-enriched M-L end-member. BB: Bual Buali, SM: Sorik Marapi, TP: Tangkuban Parahu, RB: Rajabasa.

relatively high C/N ratio of the MORB-carbonate end-member likely reflects large-scale slab C-devolatilization which enriches the overlying mantle wedge in CO_2 . Thus, the mixing relationships are consistent with carbon being derived primarily from the M-L mixture, whereas the nitrogen owes its provenance primarily to the S component.

An alternative explanation involves mixing with N-enriched carbonates in the mantle wedge (e.g., Li and Bebout, 2005). Given that calcareous diatomaceous ooze and breccia may contain up to 200 ppm N with largely positive $\delta^{15}\text{N}$ values (up to $+5\text{‰}$) (Li and Bebout, 2005) and assuming that N in the M-L end-member is mantle-like (i.e., $[\text{N}] = 1$ ppm and $\delta^{15}\text{N} = -5\text{‰}$), a simple mass balance implies that the M-L end-member can have more positive $\delta^{15}\text{N}$ values (see dashed horizontal box in Fig. 11a). However, mixing with N-enriched carbonates is not consistent with observed negative $\delta^{15}\text{N}$ values.

To further test this mixing scenario, we plot $^3\text{He}/^4\text{He}$ versus $\delta^{15}\text{N}_c$ together with end-member components MORB and sediments (see Fig. 11b caption for details). We also plot the IBVC samples for comparison and explore the role of the N-enriched M-L hybrid end-member (dashed box). Adopting a value of $5.4 R_A$ as the lower limit for He liberated from the mantle wedge (Hilton et al., 2002), we can

readily explain the data which fall above the 5.4 R_A threshold with simple binary mixing between MORB mantle and subducted sediments. Except for one sample from Bual Buali, all data from the volcanic centers can be modeled with K-values between 1 and 70 (where $K = (N/He)_S / (N/He)_M$), demonstrating the relative enrichment of the sedimentary end-member N/He values relative to that of the mantle. Indeed, we note that majority of our data can be explained with K-values between 1 and 10 which is consistent with S/M ratios in Table 3. However, samples from Tangkuban Parahu (SUM10-1) and Rajabasa (SUM10-2) require either extreme N enrichments or He deletion in the S end-member. For these 2 samples, fluids are dominated by MORB-like helium and subducted sedimentary nitrogen such that the N-enriched M-L end-member is capable of explaining the data. Interestingly, samples from the IBCV localities, in addition to one flank sample from Sorik Marapi, all of which have $^3\text{He}/^4\text{He} < 5.4 R_A$, can only be fitted with significantly lower K values (1 and less). This could suggest that they been affected by mixing with a different sedimentary end-member that has a lower $^3\text{He}/^4\text{He}$ and/or N/He ratio. We suggest that old crustal basement could have the required features (high He content due to age, and consequent low $^3\text{He}/^4\text{He}$ ratio due to radiogenic He addition) to satisfy the characteristics of such an end-member (e.g., Hilton et al., 1993).

5.4. Crustal volatile input?

Analogous to the carbon isotope system, the fundamental issue with nitrogen isotopes is that they cannot easily separate shallow crustal sediment components from deep subducted sediments as these end-members have overlapping isotopic characteristics. Thus, an alternative explanation for the C and N isotope relationships along the western Sunda arc involves assimilation and/or addition of volatiles from pre-existing crustal basements of the Sundaland crust. For example, interaction of magmatic volatiles with a crustal limestone component containing essentially no mantle-derived nitrogen, but with embedded organic nitrogen, could potentially represent the S end-members in Fig. 11a and b.

The degree of crustal contamination caused by the interaction between, or by the assimilation of, crustal volatiles can be directly addressed by $^3\text{He}/^4\text{He}$ ratios where the assimilation of crustal volatiles would be expected to lower the $^3\text{He}/^4\text{He}$ ratios. We have shown previously (Section 5.1.2.3) that the nature of the contaminant actively affecting water samples is inconsistent with a crustal limestone. Rather, the thick crustal lithologies of the Sundaland crustal core, which the magmas inevitably bypass, are likely to play a role in modifying the volatile budget of the Sumatran arc system. However, given the lack of significant radiogenic additions to the helium inventory of gas samples at volcanic centers along the arc, the effect is likely to be muted. Magmatic helium, therefore, primarily originates from the mantle wedge and reveals the presence of primordial ^3He transferred from the mantle. Those locations showing (minor) additions of radiogenic helium reveal inputs from (1) old and altered subducted oceanic crust, and/or (2) the overriding continental crust (e.g., Hilton et al., 2002). We now consider additional information from methane regarding crustal inputs to the major volatile inventory.

5.4.1. Methane–nitrogen–carbon abundance relationships

The abundance of CH_4 , and its relationship to other volatile species, are powerful tracers of shallow-level additions to the volatile inventory (Taran et al., 1998; Taran and Giggenbach, 2003). Some samples in our dataset, particularly those sampled by IBVC, contain significant CH_4 (up to ~7%, see Table 2) so can be considered to be affected by shallow-level volatile additions. Thermal decomposition of sedimentary rocks can potentially also produce N_2 , which can be readily identified by high ratios of N_2/Ar and N_2/He (Taran and Giggenbach, 2003). Therefore, hydrothermal fluids with high CH_4

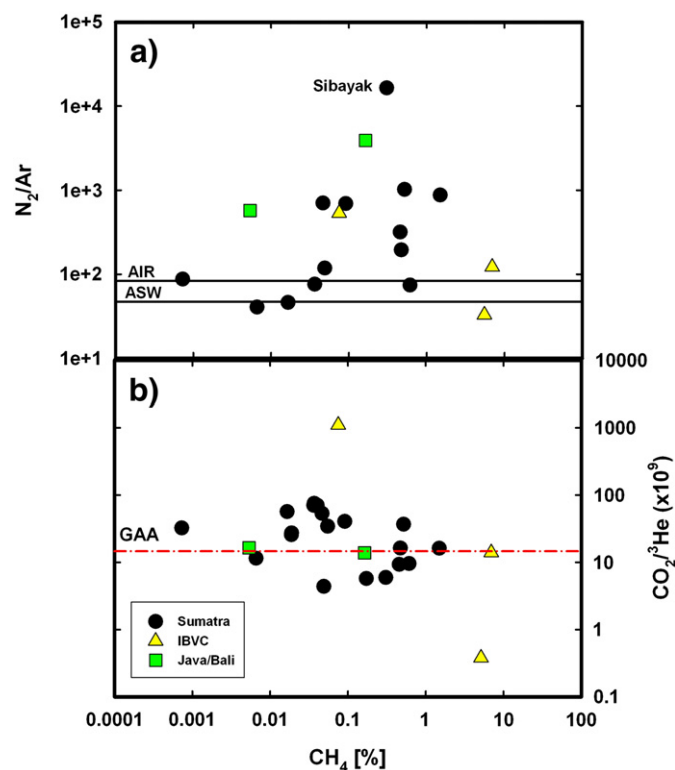


Fig. 12. a) Plot of the N_2/Ar ratio vs. CH_4 [%] content. Note that samples from Rimbo Panti and Dusan Baru (triangles), which have very high CH_4 contents, are not accompanied by high N_2/Ar ratios. Also, Sibayak has a high N_2/Ar ratio but only a modest amount of CH_4 . b) Plot of the $\text{CO}_2/{}^3\text{He}$ ratio vs. CH_4 [%] content. The lack of correlation argues against any significant shallow level additions of carbon.

content and high N_2/Ar are likely to have experienced additions of volatiles (shallow-level contamination) from organic material in the crust. This line of reasoning led Taran and Giggenbach (2003) to propose that volcanic gases and hydrothermal fluids could be distinguished by two different relationships as a reflection of their deep (volcanic) versus shallow (hydrothermal) origin. They suggested that volcanic gases from subduction zones are likely to have very little CH_4 but should be characterized by high N_2/Ar (and N_2/He) ratios as a consequence of degradation of subducted organic sediments.

To test this hypothesis, we plot N_2/Ar ratio vs. CH_4 concentration for all gas phase samples (Fig. 12a). We note that some samples with very high CH_4 content (e.g., the IBVC localities: Dusan Baru and Rimbo Panti) do not show correspondingly high N_2/Ar values despite their He isotope ratios being the lowest among our gas phase samples, suggesting that they have not sampled significant N_2 from the underlying crust. Furthermore, we do not observe any indication of a correlation between CH_4 and N_2/Ar for the remaining volcanic center samples from Sumatra and Java. For example, volcanic fluids sampled from active fumaroles at the summit of Sibayak volcano have high N_2/Ar values yet only modest CH_4 (~0.2%). This observation implies that the high N_2/Ar signal is a subducted sediment indicator rather than a crustal feature.

In Fig. 12b, we consider the relationship between $\text{CO}_2/{}^3\text{He}$ and CH_4 to assess possible crustal additions to the CO_2 budget. We note that there is no indication of a clear correlation between the CH_4 content and $\text{CO}_2/{}^3\text{He}$ for the volcanic centers and/or the IBVC localities. This observation implies that localities, such as the IBVC, which have been clearly affected by input of radiogenic helium, show insignificant addition of CO_2 during the process of crustal contamination. However, decarbonation reactions may explain high $\text{CO}_2/{}^3\text{He}$ ratios ($> 1000 \times 10^9$) in samples from one of the IBVC localities (Helatoba–Tarutung), but there is no indication in our data that such reactions produced

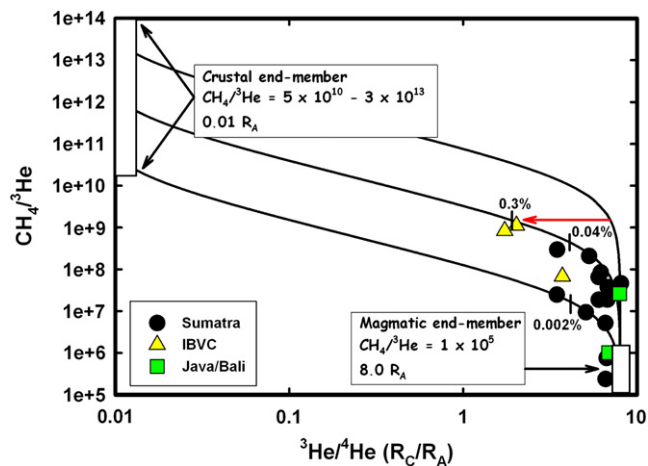


Fig. 13. Plot of $\text{CH}_4/{}^3\text{He}$ vs. helium isotopes. Solid lines indicate two-component mixing of magmatic end-member ($\text{CH}_4/{}^3\text{He} = 1.0 \times 10^5$, ${}^3\text{He}/{}^4\text{He} = 8.0R_A$) and crustal lithologies with three possible end-members compositions ($\text{CH}_4/{}^3\text{He} = 5.0 \times 10^{10}$; 1.3×10^{12} , 3.0×10^{13} with a common ${}^3\text{He}/{}^4\text{He} = 0.01R_A$). Relatively minor inputs from crustal material (<0.3%) are needed to explain the data (assuming 1.3×10^{12} as the value for the crustal end-member $\text{CH}_4/{}^3\text{He}$ ratio), including samples from the IBVC localities. The red horizontal arrow shows addition of a pure radiogenic helium crustal component from a point along the uppermost mixing line.

significant CH_4 concentrations. Thus, to conclude, the CH_4 – N_2 – CO_2 abundance relationships at the volcanic centers are inconsistent with CO_2 and N_2 being derived from shallow crustal and/or sedimentary sources. Rather, the CO_2 and N_2 primarily originate from sediment associated with the subducting sedimentary slab beneath the western Sunda arc.

5.4.2. Methane– ${}^3\text{He}$ relationships

As ${}^3\text{He}$ is predominantly derived from the mantle wedge, it can be assumed that unmodified mantle-derived gases should show fairly limited ranges in elemental ratios involving ${}^3\text{He}$. Therefore, any significant variations in ratios of CH_4 to ${}^3\text{He}$ beyond the constraints provided by MORB would suggest a non-mantle origin. In Fig. 13 we plot $\text{CH}_4/{}^3\text{He}$ vs. helium isotopes for all gas phase samples, adopting a two-component crust–mantle mixing model similar to that used by Poreda et al. (1986, 1988) and Jenden et al. (1993) for subduction zone natural gases. Since the $\text{CH}_4/{}^3\text{He}$ ratio of the crustal end-member is not well constrained, we adopt three possible end-members compositions ($\text{CH}_4/{}^3\text{He} = 5.0 \times 10^{10}$; 1.3×10^{12} , 3.0×10^{13} with a common ${}^3\text{He}/{}^4\text{He} = 0.01R_A$). For the magmatic end-member we adopt a typical upper mantle value ($\text{CH}_4/{}^3\text{He} = 1.0 \times 10^5$, ${}^3\text{He}/{}^4\text{He} = 8.0R_A$) (see also Welhan and Craig, 1983; Poreda et al., 1988; Jenden et al. 1993; Snyder et al., 2003 for discussion on possible end-member compositions).

In Fig. 13, we note the following features of the western Sunda arc data: (1) $\text{CH}_4/{}^3\text{He}$ ratios are typical of subduction zone gases, i.e., they range from $\sim 1 \times 10^6$ to 1×10^9 (Snyder et al., 2003), (2) irrespective of the crustal end-member value selected, the mixing model demonstrates the relatively minor input needed from sedimentary material to explain the overall variation in samples from the volcanic centers. In this respect, the highest crustal and/or sediment contribution (<0.3%) is evident for the IBVC localities (assuming 1.3×10^{12} as the value for the crustal end-member $\text{CH}_4/{}^3\text{He}$ ratio), and (3) a single value for the crustal end-member $\text{CH}_4/{}^3\text{He}$ ratio is inappropriate for all samples. An alternative explanation to a variable crustal end-member involves adding a pure radiogenic helium crustal component from a point along the uppermost mixing line (as shown with the red horizontal arrow in Fig. 13 - from Jenden et al., 1993). In either case, we conclude that the methane–helium relationships again point to a

minimal role of (upper) crustal contributions to the volatile inventory in the western Sunda arc.

5.5. Geological and tectonic control on the volatile budget

5.5.1. Crustal control on the volatile budget

Gasparon and Varne (1998) argued that the extent of crustal contamination increases from east to west along the Sunda arc (including Sumatra) with a concomitant diminishing role for subducted sediment influence in the petrogenesis of erupted lavas. They argued that this conclusion was consistent with increased sediment flux into the trench in the eastern part of the arc, and with the fact that large parts of the sediments are scraped off in the fore-arc region off the coast of Sumatra. The evidence presented was primarily based on profiles of radiogenic isotopes (Sr, Nd and Pb) along the Sunda arc which showed increasing radiogenic compositions to the west (see also Whitford, 1975). These results are consistent with the contrasting crustal regime between the western and eastern Sunda arc (Section 2). The Toba volcanics, and other tuffs from Sumatra, showed the highest radiogenic isotope composition in the western Sunda arc although an important caveat is that these samples may not be representative of the Sumatran arc magmas due to prolonged residence time in crustal reservoirs and consequently a large crustal signal (Chesner, 1998; Vazquez and Reid, 2004). Recently, mineral separates from the Toba volcanics have revealed a clear radiogenic helium signature ($R_A < 1.9$) (Budd et al., 2012b), supporting the notion that Toba volcanics are not useful for distinguishing between changes in crustal contamination versus mantle source contamination features along the arc, and should therefore be excluded from such comparisons due to their biased crustal signal. A similar conclusion was reached by Turner and Foden (2001).

Although crustal contamination may be more prominent in Sumatra compared to other sections of the Sunda arc, our study of volatiles in the western Sunda arc system does not support a scenario of extensive crustal controls on the volatile systematics, at least at the volcanic centers. A large number of samples of this study have only experienced relatively minor crustal contamination which only becomes significant at significant distances from the volcanic centers (i.e., IBVC localities). These results may appear somewhat surprising given the relatively thick continental crust on which most of the western Sunda arc is built. However, we note that MORB-like ${}^3\text{He}/{}^4\text{He}$ ratios ($8 \pm 1 R_A$) (Graham, 2002) as opposed to arc-like ($5.4 \pm 1.9 R_A$) (Hilton et al., 2002) are a characteristic feature of only very few samples from Sumatra whereas four out of six of our samples from Java and Bali fall within the MORB field. Again, this observation is consistent with along-arc changes in isotope signatures (e.g., Whitford, 1975; Hilton and Craig, 1989; Turner and Foden, 2001) and the contrasting crustal regimes of the Sunda arc. Furthermore, they highlight the sensitivity of helium isotopes to identify upper crustal contamination unrelated to subduction zone processes (Gasparon et al., 1994). We emphasize, however, that upper level contamination, as traced by helium isotopes, has only very minor effects on the major volatile budget for the passively-degassing volcanoes of this study. On the other hand, actively-degassing (i.e., erupting) volcanoes may enhance crustal interaction and liberate additional volatiles unrelated to the magmatic system (cf. Troll et al., 2012).

5.5.2. Subducting sedimentary control on the major volatile budget

A fundamental question regarding understanding the geochemical signatures discussed above is whether the sediments overlying the downgoing oceanic plate are subducted into the mantle or if they are simply scraped off in the fore-arc region. The Nicobar Fan off Sumatra, which constitutes the main part of the sedimentary pile, is supplied with sedimentary material (turbidite sands) from the Bengal Fan, itself derived predominantly from the uplifted Himalaya terrain, and is delivered through the Ganges–Brahmaputra river system (Curry, 1994). Owing to the presence of the structurally-high Ninety

East Ridge, most material carried to the ocean by the Meghna River is deposited west of the Ridge. These sediments are rich in quartz and chlorite-illite clay minerals (Ingersoll and Suczek, 1979), whereas in the fore-arc region off Sumatra, and adjacent to the Java segment, the sediments are mostly derived from the arc itself. They consist mainly of siliceous-clastic sediments and volcano-derived material. Based on observations from the island of Nias, off the coast of Sumatra, Moore and Curray (1980) suggested that large sections of the sediments of the incoming oceanic crust are indeed off-scraped to form the accretionary prism. These estimates are similar to independent estimates reported by Clift and Vannucchi (2004) who calculated 13% accretion efficiency (material accreted relative to material subducted) for Sumatra and 26% for Java.

Additional evidence for significant off-scraping is the lack of ^{10}Be anomalies in the Sunda arc system. ^{10}Be is a ubiquitous tracer of oceanic sediment input to arc volcanics (Morris et al., 1990) and the lack of significant ^{10}Be anomalies in Sunda arc lavas (Tera et al., 1986; Edwards et al., 1993) argues against significant recycling of late- and post Miocene sediments. In order to explain the extremely low ^{10}Be concentrations in Java volcanics, Edwards et al. (1993) argued that sediments which eventually might be related to magma generation processes in the Sunda arc are simply too old to still have active ^{10}Be . Currently, there are no ^{10}Be data available from the Sumatran subduction zone, but its main features, i.e., shallow slab dips, the relatively slow convergence rate, and the occurrence of a massive accretionary prism offshore Sumatra, make it even less likely that significant ^{10}Be anomalies will be found. Also, during off-scraping, the topmost sedimentary part is likely to be preferentially removed, thus leaving older sediments to be subducted: these sediments have very little or no active ^{10}Be remaining once they are dehydrated and eventually contribute to magma generation.

On the basis of U-series and radiogenic isotopes, Turner and Foden (2001) proposed, however, that sediment input must remain high along the Sunda arc, even though the crustal signature is most prominent in Sumatra. On the basis of our volatile data we thus favor a sedimentary, rather than crustal control, on the observed along-arc variation in the carbon systematics (Fig. 10a). In detail, we envision four potential scenarios which could explain our volatile data: 1) subducted sediments of the Nicobar Fan off Sumatra are thicker towards the source and as a result more sediments are subducting in the north (Sumatra) relative to the south (Java). This is supported by observation of Moore et al. (1980) that reported a significant increase in sediment thickness west of Java, with maximum thickness (~5 km) south of Sumatra. Furthermore, Clift and Vannucchi (2004) estimated a significant increase in material subduction rate in Sumatra ($72 \text{ km}^3/\text{my}$) compared to Java ($40 \text{ km}^3/\text{my}$), 2) more sediments are being off-scraped in the southern segment relative to northern segment, which is in agreement with observations from central Java and eastwards suggesting that very little sedimentary material enters the mantle owing to the dominance of an erosional subduction regime (Clift and Vannucchi, 2004; Kopp et al., 2006), 3) subduction of fossil spreading centers and/or oceanic plateaux and seamounts in the northeast Indian Ocean may also potentially explain these features, as they are associated with greater sediment thickness (e.g., Singh et al., 2011), 4) a sampling bias due to the fact that we have fewer samples from the south. Regardless of the exact scenario, our data support the dominant control of subducted sediments on the major volatile budget of the western Sunda arc which is in agreement with studies of other arc-systems (e.g., Varekamp et al., 1992; Sano and Marty, 1995).

6. Conclusions

A detailed study of the chemical and isotope (He–C–N) composition of volatiles associated with active fumaroles and hydrothermal fluids from passively-degassing volcanic and other centers along the

western Sunda arc has revealed the following observations. Helium isotopes at volcanic centers are consistent with the mantle wedge being the principal He contributor to the arc with only relatively minor additions of radiogenic helium from the crust, most notably on volcanic flanks and on fault-related hydrothermal systems between major volcanic centers. The CO_2 and N_2 results show considerable variation along a N–S transect of the arc, consistent with contributions from both sedimentary and mantle-derived components. However, large input of shallow crustal volatiles to the volcanic centers is not supported by $^3\text{He}/^4\text{He}$ – $\delta^{13}\text{C}$ – $\delta^{15}\text{N}$ variations or by gas chemistry (e.g., methane relationships). In this case, shallow-level crustal contamination plays only a minor role in the volatile inventory of the western Sunda arc and the subducting slab is the principal provider of volatiles. The increased contribution to the CO_2 budget from sedimentary components in the north of Sumatra likely reflect the thickening of the Nicobar Fan towards its source and consequently higher rates of material subducted in Sumatra compared to Java and Bali.

Acknowledgments

We are very grateful to Dr. Ir. A. Djumarma Wirakusumah (Geological Survey of Indonesia) for support of our 2010 field expedition. Funding for this expedition was provided by the Academic Senate (UC San Diego), discretionary funds of the Fluids and Volatiles Laboratory, Scripps Inst. Oceanography and the Swedish Science Foundation (VR), Uppsala University Centre for Natural Disaster Science (CNDS) and Otterborgska donationsfonde. The 1991 expedition was supported by Dr. Sukanto (Indonesian Geothermal Research Development Center) and funded by the German Science Foundation (DFG) and the Australian Research Council. Assistance in the field was provided by Kardana Hardjadinata, Massimo Gasparon and the late Rick Varne (1991) and Mas Majihum, Ester Jolis, Carmela Freda and David Budd (2010). Konrad Hammerschmidt (Berlin) and Bruce Deck (SIO) are thanked for laboratory assistance. Support of the SIO Fluids & Volatile Laboratory and the UNM Volcanic Fluids Laboratory is provided by the US National Science Foundation (EAR/IF-0651097 and EAR/IF-0743540, respectively). Tobias Fischer's contribution to finalizing the paper was supported by an IRD during an IPA assignment at the US National Science Foundation. Peter Barry provided useful comments on the manuscript and Joe Curray provided essential background on the Sunda arc. We thank two anonymous reviewers for their useful and constructive comments.

Appendix A. Correcting for atmosphere-derived nitrogen in $\delta^{15}\text{N}$ values

Central to the utility of nitrogen isotopes as a geochemical tracer is the assumption that the atmosphere-derived nitrogen component can be resolved from magmatic and/or sedimentary components contributing to the measured nitrogen inventory. We tested two atmosphere-correction methods, which are described in turn:

Correction based on $\delta^{15}\text{N}$ and N_2/He ratios

Following Fischer et al. (2002), the atmosphere-component can be subtracted based upon the measured N_2/He ratio. To further understand the N_2 budget of the western Sunda arc, we plot measured N_2/He vs. measured $\delta^{15}\text{N}$ for the filtered dataset along with mantle (M), sediment (S) and air end-members (A) in Fig. A1. A key advantage of this plot is that it allows visual inspection of samples which either fall within or outside the mixing envelopes defined by end-member compositions. Focusing on samples that fall within the M–S–A mixing envelope (14 out of 24 samples in the present case), we can calculate fractions derived from the N-sources for each sample. We first solve the mass balance equations of Sano et al. (1998), which describe

the relative contribution from each of these reservoirs (M, S and A) in the following manner:

$$\delta^{15}N_{obs} = f_{man} \times \delta^{15}N_{man} + f_{sed} \times \delta^{15}N_{sed} + f_{air} \times \delta^{15}N_{air} \quad (A1)$$

$$\frac{1}{(N_2/He)_{obs}} = \frac{f_{man}/(N_2/He)_{man} + f_{sed}/(N_2/He)_{sed}}{+ f_{air}/(N_2/He)_{air}} \quad (A2)$$

$$f_{man} + f_{sed} + f_{air} = 1 \quad (A3)$$

where subscripts obs = observed, man = mantle-derived, sed = sediment-derived, air = air-derived and f is the fraction for each of these end-members. Assuming that the air-derived component is not related to endogenic nitrogen so that nitrogen is derived from two sources only, it is possible to resolve the air-corrected $\delta^{15}N_c$ value into its presumed component structure using the following equation:

$$\delta^{15}N_c = f_{sed} \times \delta^{15}N_{sed} + (1 - f_{sed}) \times \delta^{15}N_{man} \quad (A4)$$

where $\delta^{15}N_c$ is the air-corrected $\delta^{15}N_c$ composition of the samples, $\delta^{15}N_{sed} = +7\%$, $\delta^{15}N_{man} = -5\%$, and f_{sed} is the fraction of sediment-derived nitrogen in a binary sediment-mantle mixture.

A clear conclusion when using this method for the western Sunda arc samples is that the sedimentary component dominates the nitrogen signature in the binary mixture. However, we also note that a significant number of data-points (10 out of 24) fall outside the mixing envelope defined by the three end-members (Fig. A1). For example, samples from Bual-Buali volcano display very low $\delta^{15}N$ values accompanied by high N_2/He . Although speculative, this observation could possibly be explained by elemental fractionation of He from N during magma degassing, due to solubility differences in melt (Lux, 1987; Libourel et al., 2003). In addition, two other localities with low N isotope values fall outside the M–A binary mixing curve (i.e., Marapi and Helatoba–Tarutung). This is similar to what has been observed previously in subduction zone fluids and has been attributed to the use of unrepresentative mantle end-member in the mixing model (Clor et al., 2005; Elkins et al., 2006; Mitchell et al., 2010). However, adoption of $\delta^{15}N$ values for the mantle end-member as low as -12% (e.g., Mohapatra and Murty, 2004) to accommodate these (outlier) samples is probably unwarranted given arguments that such low values represent experimental artifacts (Yokochi and Marty, 2006). Although we could speculate that He–N solubility differences in magmas of varying composition is the likely explanation for these samples, documented solubility data is first needed to give greater weight to this suggestion.

Correction based on air-normalized He/Ne elemental ratios

The use of the air-normalized He/Ne elemental ratios (multiplied by the ratio of the Bunsen coefficients) to correct for the presence of atmospheric-derived helium has proved successful in correcting measured helium isotope variations for air–He additions (see for example Craig, et al., 1978; Hilton, 1996).

In Fig. 3b, we plot our $\delta^{15}N$ values vs. X-values as a proxy for air contamination (see Section 4.2 and Table 1 footnote) to test the integrity of the correction for measured nitrogen isotope data. We note that if samples from the same locality do not show good agreement in measured $\delta^{15}N$ (outside the reported 1 sigma uncertainty) then values closer to the isotopic composition of air have significantly lower X-values. This applies to all duplicate measurements with the exception of summit samples from Sibayak volcano and Helatoba–Tarutung. Whether this contamination occurred in the field during sample collection and/or in the laboratory is difficult to address. Adopting methods similar to those for He isotopes, we are therefore

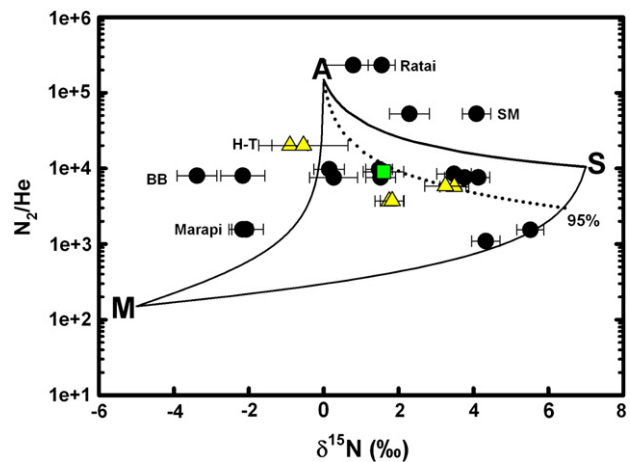


Fig. A1. Plot of N_2/He vs. $\delta^{15}N$ adopting end-members from Fischer et al. (2002), where M = mantle-derived nitrogen, S = sedimentary-derived nitrogen, and A = air-derived nitrogen. Dotted line reflects air addition to a mixture of mantle (5%) and sediment (95%) nitrogen. Samples from Bual Buali (BB), Ratai, Sorik Marapi (SM), Marapi and Helatoba–Tarutung (H–T) fall outside of the mixing envelope. Symbols as in Fig. 3.

able to correct for the presence of air N additions using the air-normalized He/Ne ratio using the following equation:

$$\delta^{15}N_c = \left[\left(\delta^{15}N_{obs} \times X \right) - 1 \right] / (X - 1) \quad (A5)$$

where X is the air-normalized He/Ne elemental ratios (see Table 1 footnote) and $\delta^{15}N_{obs}$ is the measured values. Using this methodology, we corrected the measured $\delta^{15}N$ values (reported as $\delta^{15}N$ in Table 1) to $\delta^{15}N_c$. Notably, only in the case of three samples, two water phase samples (SUM10–9 and SUM10–15) and one sample with very low X value (SUM10–25) did the corrected values differ from measured values by over 1‰ (from 1.01‰ to 1.75‰, respectively). All other corrected values agreed within 0.30‰, i.e., close to the analytical uncertainty of our $\delta^{15}N$ system. For the present dataset, another advantage of this approach is that measured $\delta^{15}N$ values $< 0\%$ (i.e., SUM10–20, SUM10–25, Cu-tube-3) correct to even lower $\delta^{15}N_c$ values as the air-derived component is subtracted. This is not possible using the N_2/He approach above as these samples fall outside the mixing envelope defined by the A–M end-members.

References

- Barry, P.H., Hilton, D.R., Halldórsson, S.A., Hahm, D., Marti, K., 2012. High precision nitrogen isotope measurements in oceanic basalts using a static triple collection noble gas mass spectrometer. *Geochemistry, Geophysics, Geosystems* 13, Q01019. <http://dx.doi.org/10.1029/2011GC003878>.
- Barry, P.H., Hilton, D.R., Fischer, T.P., de Moor, J.M., Mangasini, F., Ramirez, C.J., 2013. Helium and carbon isotope systematics of cold “mazuku” CO_2 vents and hydrothermal gases and fluids from Rungwe Volcanic Province, southern Tanzania. *Chemical Geology* 339, 141–156.
- Budd, D.A., Troll, V.R., Hilton, D.R., Freda, C., Jolis, E.M., Halldórsson, S.A., 2012a. Traversing nature’s danger zone: getting up close with Sumatra’s volcanoes. *Geology Today* 28, 64–70.
- Budd, D.A., Troll, V.R., Jolis, E.M., Deegan, F.M., Smith, V.C., Whitehouse, M.J., Harris, C., Freda, C., Hilton, D.R., Halldórsson, S.A., 2012b. Reconstructing the Toba magmatic system: insights from stable isotope geochemistry. *Goldschmidt*, abstract, Montreal.
- Cartigny, P., Ader, M., 2003. A comment to “The nitrogen record of crust–mantle interaction and mantle convection from Archean to Present” by B. Marty and N. Dauphas. *Earth and Planetary Science Letters* 216, 425–432.
- Chesner, C.A., 1998. Petrogenesis of the Toba Tuffs, Sumatra, Indonesia. *Journal of Petrology* 39, 397–438.
- Chesner, C.A., Rose, W.L., Deino, A., Drake, R., Westgate, J.A., 1991. Eruptive history of Earth’s largest Quaternary caldera (Toba, Indonesia) clarified. *Geology* 19, 200–203.
- Clift, P., Vannucchi, P., 2004. Controls on tectonic accretion versus erosion in subduction zones: implications for the origin and recycling of the continental crust. *Reviews of Geophysics* 42, RG2001. <http://dx.doi.org/10.1029/2003RG000127>.
- Clor, L.E., Fischer, T.P., Hilton, D.R., Sharp, Z.D., Hartono, U., 2005. Volatile and N isotope chemistry of the Molucca Sea collision zone: tracing source components along the

- Sangihe Arc, Indonesia. *Geochemistry, Geophysics, Geosystems* 6, Q03J14. <http://dx.doi.org/10.1029/2004GC000825>.
- Craig, H., Lupton, J.E., Horibe, Y., 1978. A mantle helium component in circum-Pacific volcanic gases: Hakone, the Marianas and Mt. Lassen. In: Alexander, E.C., Ozima, M. (Eds.), *Terrestrial Rare Gases*. Central Academic Publishers, Tokyo, pp. 3–16.
- Craig, H., Marti, K., Wiens, R., 1993. A static mass spectrometer with triple collection for nitrogen and neon isotopes. *SIO Reference Ser.*, 93–11. Scripps Inst. of Oceanogr, La Jolla, Calif, p. 1–20A.
- Curry, J.R., 1994. Sediment volume and mass beneath the Bay of Bengal. *Earth and Planetary Science Letters* 125, 371–383.
- De Leeuw, G.A., Hilton, D.R., Fischer, T.P., Walker, J.A., 2007. The He–CO₂ isotope and relative abundance characteristics of geothermal fluids in El Salvador and Honduras: new constraints on volatile mass balance of the Central American Volcanic Arc. *Earth and Planetary Science Letters* 258, 132–146.
- De Leeuw, G.A., Hilton, D.R., Güleç, N., Mutlu, H., 2010. Regional and temporal variations in CO₂³He, ³He/⁴He and $\delta^{13}\text{C}$ along the North Anatolian Fault Zone, Turkey. *Applied Geochemistry* 25, 524–539.
- Edwards, C.M.H., Morris, J.D., Thirlwall, M.F., 1993. Separating mantle from slab signatures in arc lavas using B/Be and radiogenic isotope systematics. *Nature* 362, 530–533.
- Elkins, L.J., Fischer, T.P., Hilton, D.R., Sharp, Z.D., McKnight, S., Walker, J., 2006. Tracing nitrogen in volcanic and geothermal volatiles from the Nicaraguan volcanic front. *Geochimica et Cosmochimica Acta* 70, 5215–5235.
- Fischer, T.P., Hilton, D.R., Zimmer, M.M., Shaw, A.M., Sharp, Z.D., Walker, J.A., 2002. Subduction and recycling of nitrogen along the Central American margin. *Science* 297, 1154–1157.
- Fischer, T.P., Takahata, N., Sano, Y., Sumino, H., Hilton, D.R., 2005. Nitrogen isotopes of the mantle: insights from mineral separates. *Geophysical Research Letters* 32, 2005GL022792.
- Gasparon, M., 2005. Chapter 9: Quaternary volcanicity. In: Barber, A.J., Crow, M.J., Milson, J.S. (Eds.), *Sumatra: Geology, Resources and Tectonic Evolution*. Geological Society Memoirs, 31, pp. 120–130.
- Gasparon, M., Varne, R., 1995. Sumatran granitoids and their relationship to Southeast Asian terranes. *Tectonophysics* 251, 277–299.
- Gasparon, M., Varne, R., 1998. Crustal assimilation versus subducted sediment input in west Sunda arc volcanics: an evaluation. *Mineralogy and Petrology* 64, 89–117.
- Gasparon, M., Hilton, D.R., Varne, R., 1994. Crustal contamination processes traced by helium-isotopes—examples from the Sunda Arc, Indonesia. *Earth and Planetary Science Letters* 126, 15–22.
- Gertisser, R., Keller, J., 2003. Trace element and Sr, Nd, Pb and O isotope variations in medium-K and high-K volcanic rocks from Merapi volcano, Central Java, Indonesia: evidence for the involvement of subducted sediments in Sunda arc magma genesis. *Journal of Petrology* 44 (3), 457–489.
- Giggenbach, W.F., 1996. Chemical composition of volcanic gases. In: Scarpa, R., Tilling, R. (Eds.), *Monitoring and Mitigation of Volcanic Hazards*. Springer, pp. 221–256.
- Graham, D.W., 2002. Noble gas isotope geochemistry of mid-ocean ridge and ocean island basalts: characterization of mantle source reservoirs. In: Porcelli, D., Ballentine, C.J., Wieler, R. (Eds.), *Noble Gases in Geochemistry and Cosmochemistry*. Rev. Mineral. Geochem., vol. 47. Mineral. Soc. Am, Washington, DC, pp. 247–317.
- Hamilton, W., 1979. Tectonics of the Indonesian region. *U.S. Geol. Surv. Prof. Pap.*, 1078, 345 pp.
- Hilton, D.R., 1996. The helium and carbon isotope systematics of a continental geothermal system: result from monitoring studies at Long Valley caldera (California, U.S.A.). *Chemical Geology* 127, 269–295.
- Hilton, D.R., Craig, H., 1989. A helium isotope transect along the Indonesian archipelago. *Nature* 342, 906–908.
- Hilton, D.R., Hammerschmidt, K., Teufel, S., Friedrichsen, H., 1993. Helium isotope characteristics of Andean geothermal fluids and lavas. *Earth and Planetary Science Letters* 120, 265–282.
- Hilton, D.R., Gronvold, K., Sveinbjornsdottir, A., Hammerschmidt, K., 1998a. Helium isotope evidence for off-axis degassing of the Icelandic hotspot. *Chemical Geology* 149, 173–187.
- Hilton, D.R., McMurtry, G.M., Goff, F., 1998b. Large variations in vent fluid CO₂³He ratios signal rapid changes in magma chemistry at Loihi Seamount, Hawaii. *Nature* 396, 359–362.
- Hilton, D.R., Fischer, T.P., Marty, B., 2002. Noble gases and volatile recycling at subduction zones. In: Porcelli, D., Ballentine, C.J., Wieler, R. (Eds.), *Noble Gases in Geochemistry and Cosmochemistry*. Rev. Mineral. Geochem., vol. 47. Mineral. Soc. Am, Washington, DC, pp. 319–370.
- Holloway, J.R., Blank, J.G., 1994. Application of experimental results to C–O–H species in natural melts. In: Carrol, M.R., Holloway, J. (Eds.), *Volatiles in Magmas*. Rev. Mineral. Geochem., vol. 30. Mineral. Soc. Am, Washington, DC, pp. 187–230.
- Ingersoll, R.V., Sucek, C.A., 1979. Petrology and provenance of Neogene sand from Nicobar and Bengal fans, DSDP sites 211 and 218. *Journal of Sedimentary Petrology* 49, 1217–1228.
- Inguaggiato, S., Taran, Y., Grassa, F., Capasso, G., Favara, R., Varley, N., Faber, E., 2004. Nitrogen isotopes in thermal fluids of a forearc region (Jalisco Block, Mexico): evidence for heavy nitrogen from continental crust. *Geochemistry, Geophysics, Geosystems* 5, Q12003. <http://dx.doi.org/10.1029/2004GC000767>.
- Jenden, P.D., Hilton, D.R., Kaplan, I.R., Craig, H., 1993. Abiogenic hydrocarbons and mantle helium in oil and gas fields. In: Howell, D.G. (Ed.), *The Future of Energy Gases*: USGS. Prof. Paper, 1570, pp. 31–56.
- Kopp, H., Flueh, E.R., Petersen, C.J., Weinrebe, W., Wittwer, A., Meramex Scientists, 2006. The Java margin revisited: evidence for subduction erosion off Java. *Earth and Planetary Science Letters* 242, 130–142.
- Li, L., Bebout, G.E., 2005. Carbon and nitrogen geochemistry of sediments in the Central American convergent margin: insights regarding subduction input fluxes, diagenesis and paleoproductivity. *Journal of Geophysical Research* 110, B11202. <http://dx.doi.org/10.1029/2004JB003276>.
- Li, L., Bebout, G.E., Idleman, B.D., 2007. Nitrogen concentration and $\delta^{15}\text{N}$ of altered oceanic crust obtained on ODP Legs 129 and 185: insights into alteration-related nitrogen enrichment and the nitrogen subduction budget. *Geochimica et Cosmochimica Acta* 71, 2344–2360.
- Li, L., Cartigny, P., Ader, M., 2009. Kinetic nitrogen isotope fractionation associated with thermal decomposition of NH₃: experimental results and potential implications to natural-gas and hydrothermal systems. *Geochimica et Cosmochimica Acta* 73, 6282–6297.
- Libourel, G., Marty, B., Humbert, F., 2003. Nitrogen solubility in basaltic melt. Part I. Effect of oxygen fugacity. *Geochimica et Cosmochimica Acta* 67, 4123–4135.
- Lux, G., 1987. The behavior of noble gases in silicate liquids: solution, diffusion, bubbles and surface effects, with applications to natural samples. *Geochimica et Cosmochimica Acta* 51, 1549–1560.
- Marty, B., Dauphas, N., 2003a. The nitrogen record of crust–mantle interaction and mantle convection from Archean to Present. *Earth and Planetary Science Letters* 206, 397–410.
- Marty, B., Dauphas, N., 2003b. “Nitrogen isotopic compositions of the present mantle and the Archean biosphere”: reply to comment by Pierre Cartigny and Magali Ader. *Earth and Planetary Science Letters* 216, 433–439.
- Marty, B., Jambon, A., 1987. C³He in volatile fluxes from the solid Earth: implication for carbon geodynamics. *Earth and Planetary Science Letters* 83, 16–26.
- Marty, B., Jambon, A., Sano, Y., 1989. Helium isotopes and CO₂ in volcanic gases of Japan. *Chemical Geology* 76, 25–40.
- Mattey, D.P., 1991. Carbon dioxide solubility and carbon isotope fractionation in basaltic melt. *Geochimica et Cosmochimica Acta* 55, 3467–3473.
- McCaffrey, R., 2009. The tectonic framework of the Sumatran Subduction Zone. *Annual Reviews of Earth and Planetary Sciences*, 37, pp. 345–366.
- Mitchell, E.C., Fischer, T.P., Hilton, D.R., Hauri, E.H., Shaw, A.M., de Moor, J.M., Sharp, Z.D., Kazahaya, K., 2010. Nitrogen sources and recycling at subduction zones: insights from the Izu–Bonin–Mariana Arc. *Geochemistry, Geophysics, Geosystems* 11, Q02X11. <http://dx.doi.org/10.1029/2009GC002783>.
- Mohapatra, R.K., Murty, S.V.S., 2004. Nitrogen isotopic composition of the MORB mantle: a reevaluation. *Geochemistry, Geophysics, Geosystems* 5, Q01001. <http://dx.doi.org/10.1029/2003GC000612>.
- Moore, G.F., Curry, J.R., 1980. Structure of the Sunda Trench lower slope west of Sumatra from multichannel seismic reflection data. *Marine Geophysical Researches* 4, 319–340.
- Moore, G.F., Curry, J.R., Moore, D.G., Karig, D.E., 1980. Variations in deformation along the Sunda forearc, northeast Indian Ocean. In: Hayes, D.E. (Ed.), *Geophys. Monograph*. The tectonic and geologic evolution of Southeast Asian seas and islands: Geoph. Mon., vol. 23, pp. 145–160.
- Morris, J.D., Leeman, W.P., Tera, F., 1990. The subducted component in island arc lavas: constraints from Be isotopes and B–Be systematics. *Nature* 344, 31–36.
- Ozima, M., Podosek, F.A., 2002. *Noble Gas Geochemistry*, 2nd ed. Cambridge Univ. Press, New York, 286 pp.
- Peters, K.E., Sweeny, R.E., Kaplan, I.R., 1978. Correlation of carbon and nitrogen stable isotope ratios in sedimentary organic matter. *Limnology and Oceanography* 23, 598–604.
- Poreda, R., Craig, H., 1989. Helium isotope ratios in circum-Pacific volcanic arcs. *Nature* 338, 473–478.
- Poreda, R.J., Jenden, P.D., Kaplan, I.R., Craig, H., 1986. Mantle helium in Sacramento basin natural gas wells. *Geochimica et Cosmochimica Acta* 50, 2847–2853.
- Poreda, R.J., Jeffrey, A.W.A., Kaplan, I.R., Craig, H., 1988. Magmatic helium in subduction zone natural gases. *Chemical Geology* 71, 199–210.
- Ray, M.C., Hilton, D.R., Munoz, J., Fischer, T.P., Shaw, A.M., 2009. The effects of volatile recycling, degassing and crustal contamination on the helium and carbon geochemistry of hydrothermal fluids from the Southern Volcanic Zone of Chile. *Chemical Geology* 266, 38–49.
- Sadofsky, S.J., Bebout, G.E., 2004. Nitrogen geochemistry of subducting sediments: new results from the Izu–Bonin–Mariana margin and insights regarding global nitrogen subduction. *Geochemistry, Geophysics, Geosystems* 5, Q03115. <http://dx.doi.org/10.1029/2003GC000543>.
- Sano, Y., Marty, B., 1995. Origin of carbon in fumarolic gas from island arcs. *Chemical Geology* 119, 265–274. [http://dx.doi.org/10.1016/0009-2541\(94\)00097-R](http://dx.doi.org/10.1016/0009-2541(94)00097-R).
- Sano, Y., Williams, S.N., 1996. Fluxes of mantle and subducted carbon along convergent plate boundaries. *Geophysical Research Letters* 23, 2749–2752.
- Sano, Y., Nakamura, Y., Wakita, H., Urabe, A., Tominaga, Y., 1984. ³He emission related to volcanic activity. *Science* 224, 150–151.
- Sano, Y., Takahata, N., Nishio, Y., Marty, B., 1998. Nitrogen recycling in subduction zones. *Geophysical Research Letters* 25, 2289–2292.
- Shaw, A.M., Hilton, D.R., Fischer, T.P., Walker, J.A., Alvarado, G., 2003. Helium and carbon relationships in geothermal fluids from the Central American arc in Costa Rica. *Earth and Planetary Science Letters* 214, 499–513.
- Shilobreeva, S., Martinez, I., Busigny, V., Agrinier, P., Laverne, C., 2011. Insights into C and H storage in the altered oceanic crust: results from ODP/IODP Hole 1256D. *Geochimica et Cosmochimica Acta* 75, 2237–2255.
- Sieh, K., Natawidjaja, D., 2000. Neotectonics of the Sumatran fault, Indonesia. *Journal of Geophysical Research* 105, 28295–28326.
- Singh, S.C., et al., 2011. Aseismic zone and earthquake segmentation associated with a deep subducted seamount in Sumatra. *Nature Geoscience* 5, 308–311.
- Smithsonian Institution, 2011. Marapi. *Bulletin of the Global Volcanism Network* 36 (7).
- Smyth, H.R., Hamilton, P.J., Hall, R., Kinney, P.D., 2007. The deep crust beneath island arcs: inherited zircons reveal a Gondwana continental fragment beneath East Java, Indonesia. *Earth and Planetary Science Letters* 258, 269–282.

- Snyder, G., Poreda, R., Fehn, U., Hunt, A., 2003. Sources of nitrogen and methane in Central American geothermal settings: noble gas and ^{129}I evidence for crustal and magmatic volatile components. *Geochemistry, Geophysics, Geosystems* 4 (1), 9001. <http://dx.doi.org/10.1029/2002GC000363>.
- Szaran, J., 1997. Achievement of carbon isotope equilibrium in the system HCO_3^- (solution)– CO_2 (gas). *Chemical Geology* 142, 79–86.
- Taran, Y.A., Giggenbach, W.F., 2003. Geochemistry of light hydrocarbons in volcanic and hydrothermal fluids. Society of Economic Geologists Special Publication, 10, pp. 61–74.
- Taran, Y., Fischer, T.P., Porovsky, B., Sano, Y., Armentia, M.A., Macias, J.L., 1998. Geochemistry of the volcano-hydrothermal system of El Chichón volcano, Chiapas Mexico. *Bulletin of Volcanology* 59, 436–449.
- Tera, F., Brown, L., Morris, J., Sacks, I.S., Klein, J., Middleton, R., 1986. Sediment incorporation in island-arc magmas: inferences from ^{10}Be . *Geochimica et Cosmochimica Acta* 50, 535–550.
- Troll, V.R., Hilton, D.R., Jolis, E.M., Chadwick, J.P., Blythe, L.S., Deegan, F.M., Schwarzkopf, L.M., Zimmer, M., 2012. Crustal CO_2 liberation during the 2006 eruption and earthquake events at Merapi volcano Indonesia. *Geophysical Research Letters* 39, L11302. <http://dx.doi.org/10.1029/2012GL051307>.
- Turner, S., Foden, J., 2001. U–Th–Ra disequilibria. Sr–Nd–Pb isotope and trace element variations in Sunda arc lavas: predominance of a subducted sediment component. *Contributions to Mineralogy and Petrology* 142, 43–57.
- van Soest, M.C., Hilton, D.R., Kreulen, R., 1998. Tracing crustal and slab contributions to arc magmatism in the Lesser Antilles island arc using helium and carbon relationships in geothermal fluids. *Geochimica et Cosmochimica Acta* 62, 3323–3335.
- Varekamp, J.C., Kreulen, R., Poorter, R.P.E., van Bergen, M.J., 1992. Carbon sources in arc volcanism with implications for the carbon cycle. *Terra Nova* 4, 363–373.
- Vazquez, J.A., Reid, M.R., 2004. Probing the accumulation history of the voluminous Toba magma. *Science* 305, 991–994.
- von Huene, R., Scholl, D.W., 1991. Observations at convergent margins concerning sediment subduction, subduction erosion, and the growth of continental crust. *Reviews of Geophysics* 29, 279–316.
- Weiss, R.F., 1971. Solubility of helium and neon in water and seawater. *Journal of Chemical & Engineering Data* 16, 235–241.
- Weiss, R.F., 1974. Carbon dioxide in water and seawater: the solubility of a non-ideal gas. *Marine Chemistry* 2, 203–215.
- Welhan, J.A., Craig, H., 1983. Methane, hydrogen and helium in hydrothermal fluids at 21°N on the East Pacific Rise. In: Rona, P.A., Bostrom, K., Laubier, L., Smith, K.L. (Eds.), *Hydrothermal Processes at Seafloor Spreading Centers*. Plenum Press, New York, pp. 391–409.
- Whitford, D.J., 1975. Strontium isotopic studies of the volcanic rocks of the Sunda arc, Indonesia, and their petrogenetic implications. *Geochimica et Cosmochimica Acta* 39, 1287–1302.
- Whitford, D.J., 1981. Neodymium isotopic composition of Quaternary island arc lavas from Indonesia. *Geochimica et Cosmochimica Acta* 45, 989–995.
- Widiyantoro, S., van der Hilst, R., 1996. Structure and evolution of lithospheric slab beneath the Sunda Arc, Indonesia. *Science* 271, 1566–1570.
- Yokochi, R., Marty, B., 2006. Fast chemical and isotopic exchange of nitrogen during reaction with hot molybdenum. *Geochemistry, Geophysics, Geosystems* 7, Q07004. <http://dx.doi.org/10.1029/2006GC001253>.
- Zimmer, M.M., Fischer, T.P., Hilton, D.R., Alvarado, G.E., Sharp, Z.D., Walker, J.A., 2004. Nitrogen systematics and gas fluxes of subduction zones: insights from Costa Rica arc volatiles. *Geochemistry, Geophysics, Geosystems* 5. <http://dx.doi.org/10.1029/2003GC000651>.